

**Journal of Geophysical Research: Atmospheres****RESEARCH ARTICLE**

10.1002/2015JD024273

**Special Section:**

Deep Convective Clouds and Chemistry 2012 Studies (DC3)

This article is a companion to Huntrieser et al. [2016] doi:10.1002/2015JD024279.

**Key Points:**

- Severe overshooting Central U.S. thunderstorms probed in situ by three aircraft
- Highly variable NO<sub>x</sub> and O<sub>3</sub> mixing ratios in the anvil outflow region
- Mixing of lightning-produced NO<sub>x</sub> and O<sub>3</sub>-rich stratospheric air masses

**Correspondence to:**H. Huntrieser,  
Heidi.Huntrieser@dlr.de**Citation:**

Huntrieser, H., et al. (2016), Injection of lightning-produced NO<sub>x</sub>, water vapor, wildfire emissions, and stratospheric air to the UT/LS as observed from DC3 measurements, *J. Geophys. Res. Atmos.*, 121, 6638–6668, doi:10.1002/2015JD024273.

Received 25 SEP 2015

Accepted 28 MAR 2016

Accepted article online 1 APR 2016

Published online 11 JUN 2016

**Injection of lightning-produced NO<sub>x</sub>, water vapor, wildfire emissions, and stratospheric air to the UT/LS as observed from DC3 measurements**

**H. Huntrieser<sup>1</sup>, M. Lichtenstern<sup>1</sup>, M. Scheibe<sup>1</sup>, H. Aufmhoff<sup>1</sup>, H. Schlager<sup>1</sup>, T. Pucik<sup>1,2</sup>, A. Minikin<sup>1</sup>, B. Weinzierl<sup>1,3</sup>, K. Heimerl<sup>1</sup>, I. B. Pollack<sup>4,5,6</sup>, J. Peischl<sup>4,5</sup>, T. B. Ryerson<sup>4</sup>, A. J. Weinheimer<sup>7</sup>, S. Honomichl<sup>7</sup>, B. A. Ridley<sup>7</sup>, M. I. Biggerstaff<sup>8</sup>, D. P. Betten<sup>8</sup>, J. W. Hair<sup>9</sup>, C. F. Butler<sup>9</sup>, M. J. Schwartz<sup>10</sup>, and M. C. Barth<sup>7</sup>**

<sup>1</sup>Deutsches Zentrum für Luft- und Raumfahrt, Institut für Physik der Atmosphäre, Oberpfaffenhofen, Germany, <sup>2</sup>Masaryk University, Brno, Czech Republic, <sup>3</sup>Faculty of Physics, University of Vienna, Vienna, Austria, <sup>4</sup>NOAA, Boulder, Colorado, USA, <sup>5</sup>CIRES, University of Colorado Boulder, Boulder, Colorado, USA, <sup>6</sup>Now at Atmospheric Science Department, Colorado State University, Fort Collins, Colorado, USA, <sup>7</sup>NCAR, Boulder, Colorado, USA, <sup>8</sup>School of Meteorology, University of Oklahoma, Norman, Oklahoma, USA, <sup>9</sup>NASA Langley Research Center, Hampton, Virginia, USA, <sup>10</sup>Jet Propulsion Laboratory, California Institute of Technology, Pasadena, California, USA

**Abstract** During the Deep Convective Clouds and Chemistry (DC3) experiment in summer 2012, airborne measurements were performed in the anvil inflow/outflow of thunderstorms over the Central U.S. by three research aircraft. A general overview of Deutsches Zentrum für Luft- und Raumfahrt (DLR)-Falcon in situ measurements (CO, O<sub>3</sub>, SO<sub>2</sub>, CH<sub>4</sub>, NO, NO<sub>x</sub>, and black carbon) is presented. In addition, a joint flight on 29 May 2012 in a convective line of isolated supercell storms over Oklahoma is described based on Falcon, National Science Foundation/National Center for Atmospheric Research Gulfstream-V (NSF/NCAR-GV), and NASA-DC8 trace species in situ and lidar measurements. During DC3 some of the largest and most destructive wildfires in New Mexico and Colorado state's history were burning, which strongly influenced air quality in the DC3 thunderstorm inflow and outflow region. Lofted biomass burning (BB) plumes were frequently observed in the mid- and upper troposphere (UT) in the vicinity of deep convection. The impact of lightning-produced NO<sub>x</sub> (LNO<sub>x</sub>) and BB emissions was analyzed on the basis of mean vertical profiles and tracer-tracer correlations (CO-NO<sub>x</sub> and O<sub>3</sub>-NO). On a regular basis DC3 thunderstorms penetrated the tropopause and injected large amounts of LNO<sub>x</sub> into the lower stratosphere (LS). Inside convection, low O<sub>3</sub> air ( $\sim 80 \text{ nmol mol}^{-1}$ ) from the lower troposphere was rapidly transported to the UT/LS region. Simultaneously, O<sub>3</sub>-rich stratospheric air masses ( $\sim 100\text{--}200 \text{ nmol mol}^{-1}$ ) were present around and below the thunderstorm outflow and enhanced UT-O<sub>3</sub> mixing ratios significantly. A 10 year global climatology of H<sub>2</sub>O data from the Aura Microwave Limb Sounder confirmed that the Central U.S. is a preferred region for convective injection into the LS.

**1. Introduction**

Thunderstorms and lightning are known to redistribute and produce chemical constituents within the troposphere [Dickerson et al., 1987; Huntrieser et al., 1998, 2012]. Especially, the upper tropospheric budgets of ozone (O<sub>3</sub>) and nitrogen oxides (NO<sub>x</sub> ≈ NO + NO<sub>2</sub>) are significantly affected by deep convection. There is a need for a more comprehensive understanding of these processes and their effect on O<sub>3</sub> which plays a key role in the chemistry and acts as a prominent greenhouse gas at these altitudes [Myhre et al., 2013].

The main sources of tropospheric ozone are photochemical production and downward transport (entrainment) of O<sub>3</sub>-rich air from the stratosphere [Crutzen, 1995; Stevenson et al., 2006]. A variety of natural and anthropogenic sources in the boundary layer (BL) (e.g., wildfires and fossil fuel combustion) emit large amounts of ozone precursors, such as carbon monoxide (CO), methane (CH<sub>4</sub>), NO<sub>x</sub>, and volatile organic compounds (VOCs). These emissions can be uplifted to the upper troposphere (UT) by warm conveyor belts and/or deep convection embedded in frontal systems [Cooper et al., 2004]. In addition, further emission sources in the UT originate from lightning-produced NO<sub>x</sub> (LNO<sub>x</sub>) ( $5 \pm 3 \text{ Tg a}^{-1}$ ) and aircraft [Schumann and Huntrieser, 2007]. Ozone is produced in the troposphere by photochemical oxidation of these precursors in the presence of hydrogen oxides (HO<sub>x</sub> ≈ HO + HO<sub>2</sub>) and NO [Crutzen, 1970; Fishman et al., 1979].

Ozone in the UT has been estimated to be enhanced globally by 12% due to the net effect of convective transport of O<sub>3</sub> and its precursors [Lawrence *et al.*, 2003]. In contrast, Doherty *et al.* [2005] found a reduction in UT-O<sub>3</sub> of similar magnitude (13%) caused by convective transport of low O<sub>3</sub> air from the lower troposphere. Lawrence and Rasch [2005] showed that differences in the tracer transport may be caused by the applied convective mass flux scheme. Besides vertical transport and photochemical processes in lofted polluted air masses, LNO<sub>x</sub> is an important natural O<sub>3</sub> precursor in the UT. Compared to the boundary layer (BL), where the lifetime of NO<sub>x</sub> is only a few hours, the lifetime in the UT increases to ~2–3 days [Ehhalt and Rohrer, 1995]. During airborne field experiments [e.g., Huntrieser *et al.*, 2002] aged upper tropospheric thunderstorm outflow has been observed ~1–2 days after the main convective activity; however, its effect on the O<sub>3</sub> budget at these altitudes is still not well understood.

Furthermore, simulations with global models over North America (NA) in summer have shown large discrepancies in quantifying UT-O<sub>3</sub> and UT-NO<sub>x</sub> produced by lightning compared to observations [Pfister *et al.*, 2008; Cooper *et al.*, 2009; Hudman *et al.*, 2009; Allen *et al.*, 2010; Jourdain *et al.*, 2010]. Recently, Wang *et al.* [2013] pointed out that present model predictions for UT-O<sub>3</sub> over NA are generally too low and still differ by ~20–25 nmol mol<sup>-1</sup> compared to measurements with ozonesondes.

The overall aim of the present and a follow-up study [Huntrieser *et al.*, 2016] is to contribute to the important scientific tasks described above and to give further evidence from an airborne field experiment that thunderstorms over the Central United States (U.S.) may play an even larger role in the upper tropospheric and lower stratospheric NO<sub>x</sub> and O<sub>3</sub> budgets than previously thought.

From previous studies it is known that intense thunderstorms may penetrate the tropopause region. Evidence from aircraft and satellite observations of extratropical convection injecting BL into the lowermost stratosphere has been reported in several studies [Roach, 1967; Poulida *et al.*, 1996; Fischer *et al.*, 2003; Dessler and Sherwood, 2004; Hegglin *et al.*, 2004; Ray *et al.*, 2004; Anderson *et al.*, 2012; Homeyer *et al.*, 2014]. Based on detailed observations in one overshooting mesoscale convective complex (MCC) over North Dakota, Poulida *et al.* [1996] stated that MCCs may contribute more to the stratosphere-troposphere exchange than assumed. Stenchikov *et al.* [1996] concluded that if the investigated MCC is typical of the ~100 MCCs occurring annually at midlatitudes, this transport mechanism may play an essential role for O<sub>3</sub>, NO<sub>y</sub>, and CO budgets in the UT/lower stratosphere (LS) region and is probably the most important source of water vapor (H<sub>2</sub>O) at these altitudes in the extratropics. Observations by Wang [2003] and more recently by Anderson *et al.* [2012] indicate that a high frequency of the deep convective events in midlatitudes may penetrate into the lowermost stratosphere (LMS), which significantly impacts the H<sub>2</sub>O budget in this region. Evidence for this transport process was found in ~50% of Anderson *et al.* flights over North America.

The findings summarized above show that the dynamics and chemistry in deep convection are very complex processes that have a large impact on the composition of trace species in the UT/LS region. There is a need for a more comprehensive understanding of these processes and their effect on the O<sub>3</sub> budget.

The objective of the Deep Convective Clouds and Chemistry Project (DC3) experiment presented here was to investigate midlatitude deep convection in large detail by a variety of different instruments [Barth *et al.*, 2015]. The idea was to study dynamical, physical, and electrical processes, as well as the effect of deep convection on the chemical composition in the UT/LS region simultaneously. Previous thunderstorm experiments as the "Stratosphere-Troposphere Experiment: Radiation, Aerosol, and Ozone" (STERAO-A) campaign in 1996 over Colorado and the "Cirrus Regional Study of Tropical Anvils and Cirrus Layers-Florida Area Cirrus Experiment" (CRYSTAL-FACE) in 2002 over Florida [Dye *et al.*, 2000; Ridley *et al.*, 2004] focused either more on chemistry or more on dynamical/physical/electrical processes as described in Barth *et al.* [2015]. For reasons mentioned above and below, the Central U.S. was selected as a suitable operation area for DC3. Recent global satellite measurements indicate that thunderstorms over the Central and southeastern U.S. are among the strongest on Earth producing especially large hail and high overshooting cloud tops reaching into the LMS [Cecil, 2011; Cecil and Blankenship, 2012; Schwartz *et al.*, 2013]. The lightning stroke density is also very high in this region [Holle and Murphy, 2015; Virts *et al.*, 2015].

During the DC3 experiment in summer 2012, a more pronounced interaction between thunderstorms and stratospheric air masses was observed than reported from previous U.S. experiments as STERAO-A and CRYSTAL-FACE. For example Pan *et al.* [2014] presented first evidences in lidar images of downward transport

of O<sub>3</sub>-rich air masses from the stratosphere wrapped around the anvil outflow of a mesoscale convective system (MCS). Further recent evidence of mixing between polluted convective outflow and stratospheric air masses during DC3 has been presented by *Schroeder et al.* [2014].

Furthermore, during DC3 some of the largest and most destructive wildfires in New Mexico and Colorado state's history were burning, which strongly influenced air quality in the DC3 thunderstorm inflow and outflow region (presented here) and the lightning frequency [*Lang et al.*, 2014]. It is known that smoke particles can efficiently be transported to the UT by deep convection and contribute to the intensification of thunderstorms and lightning frequency due to an increased number of smaller ice particles transported to higher altitudes [*Lyons et al.*, 1998; *Murray et al.*, 2000; *Andreae et al.*, 2001, 2004; *Yuan et al.*, 2011]. Furthermore, it is known that the convective transport of biomass burning emissions may produce significant amounts of O<sub>3</sub> [*Pickering et al.*, 1996].

In the present study we introduce a unique set of new measurements obtained from the DC3 field experiment. The analyses are divided into two parts, as described in more detail in the next paragraph; a general overview of our measurements is given in the present paper, and more detailed analyses follow in HH2016 (which refers to *Huntrieser et al.* [2016]).

Here we report on airborne in situ measurements carried out by two U.S. and one German research aircraft. Our analyses focus on a number of trace species, such as sulphur dioxide (SO<sub>2</sub>), CO, O<sub>3</sub>, CH<sub>4</sub>, NO, NO<sub>x</sub>, and refractory black carbon (rBC) measured in situ by the latter aircraft, a Falcon-20 of the Deutsches Zentrum für Luft- und Raumfahrt (DLR). The analyses are based on mean vertical profiles of a variety of trace species and tracer-tracer correlations (CO-NO<sub>x</sub> and O<sub>3</sub>-NO) to give an overview of the Falcon measurements. The primary objective is to study emissions from wildfires and LNO<sub>x</sub> within and in the vicinity of the fresh thunderstorm outflow. Independently of the DC3 field experiment, a data set containing Aura Microwave Limb Sounder (MLS) water vapor measurements is analyzed to study the general impact of deep convection during DC3 on the lowermost stratosphere compared to other regions. The stratosphere-troposphere exchange of O<sub>3</sub> and H<sub>2</sub>O is touched upon. Finally, a case study (joint Falcon flight with DC8 and Gulfstream-V (GV)) is presented focusing on a severe convection case on 29 May 2012 over Texas/Oklahoma where deep convective clouds with overshooting tops developed. The secondary objective in the present study is to analyze the dynamics of this storm system and its impact on the O<sub>3</sub> and aerosol composition in the UT/LS region. In contrast, HH2016 presents detailed analyses based on three Falcon case studies with the main focus on the O<sub>3</sub> distribution within and in the vicinity of the fresh and aged thunderstorm outflow.

The DC3 field experiment design and meteorological situation, the airborne trace gas instrumentation on board of the Falcon, selected flight planning tools and postanalysis products are described in section 2. A general overview of Falcon observations during DC3 impacted by emissions from wildfires and LNO<sub>x</sub> is given in section 3. Evidence of convective injection into the lowermost stratosphere of LNO<sub>x</sub> and H<sub>2</sub>O is discussed in section 4. A case study focusing on the fresh anvil outflow from a severe convective line over Texas/Oklahoma on 29 May 2012 and its impact on the aerosol and O<sub>3</sub> composition in the UT/LS region is presented in section 5. A summary, discussion, and conclusions are given in section 6.

## 2. DC3 Mission Design and Data Products

### 2.1. DC3 Field Experiment and Meteorological Situation

The DC3 project ([https://www.eol.ucar.edu/field\\_projects/dc3](https://www.eol.ucar.edu/field_projects/dc3)) was initiated by the National Center for Atmospheric Research (NCAR), the U.S. university community, the National Aeronautics and Space Administration (NASA), and the National Oceanic and Atmospheric Administration (NOAA). A detailed overview of the DC3 field experiment is given by *Barth et al.* [2015]. From 1 May to 30 June 2012 the field phase was carried out mainly targeting thunderstorms over Texas/Oklahoma, Colorado, and Alabama. All three operating research aircraft, the National Science Foundation/National Center for Atmospheric Research Gulfstream-V (NSF/NCAR Gulfstream-V (GV)), NASA-DC8, and DLR-Falcon were based at the airport in Salina, Kansas (38.8°N, 97.6°W). The German aircraft operated in Salina from 27 May to 17 June. Ground-based radar networks and lightning mapping arrays complemented the aircraft measurements with electrical, physical, and kinematic characteristics of the storms.

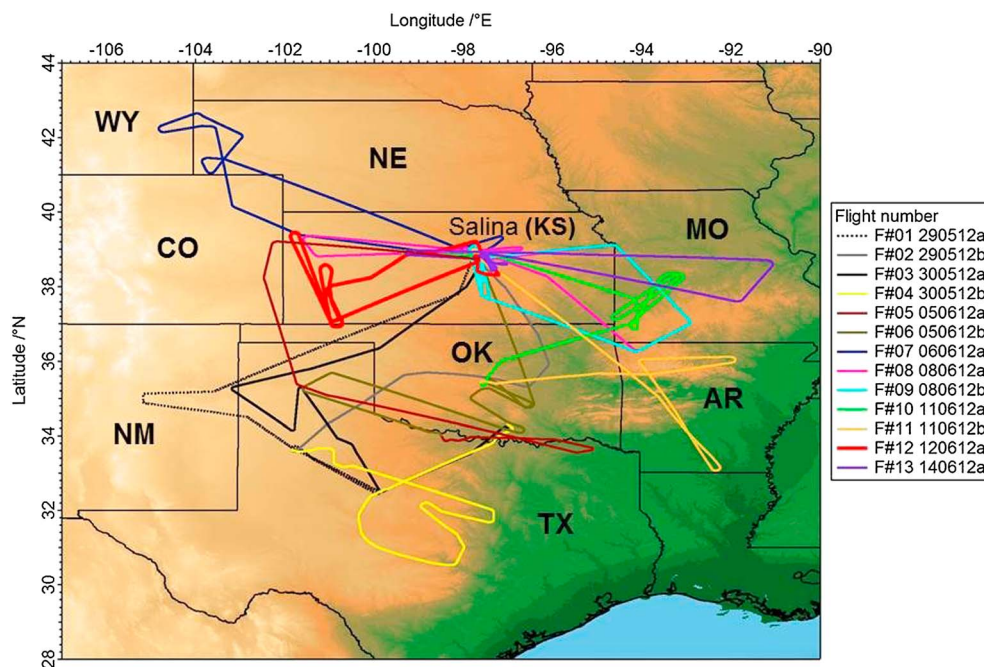


**Figure 1.** Thirteen Falcon flights were performed over the Central U.S. during DC3 from the operation site in Salina (KS). The flights are color coded according to date and flight number as listed in the legend.

The main objective of the Falcon and GV aircraft was to study the fresh and aged high-altitude outflow from thunderstorms, whereas the DC8 aircraft focused on the low-altitude thunderstorm inflow region and provided remote sensing observations to guide the other aircraft during the flights. After completing the low-level inflow sampling, the DC-8 also often sampled convective outflow in the UT. The main features observed during all DC3 flights are summarized by Barth *et al.* [2015, Table 5].

All aircraft were equipped with a variety of instruments to measure trace species, radiation, and cloud particle characteristics [see Barth *et al.*, 2015, Tables 2–4]. The performance of similar instruments on different aircraft was tested during several intercomparison flights (wingtip-to-wingtip formation). More details on the Falcon instrumentation and its performance are presented in section 2.2.

The overarching goal of DC3 was to sample thunderstorms in a coordinated fashion in conjunction with the ground-based observations. The Falcon flew in the same storm systems as the U.S. aircraft during three missions (29 May and 6 and 11 June) but was slightly separated in time and/or space [see Barth *et al.*, 2015, Table 5]. Limiting factors for the Falcon aircraft were its maximum flight duration and altitude of 3.5 h and 12.4 km, respectively. Since the targeted thunderstorms were located at a far distance from the aircraft base in Salina, the Falcon often made at least one stop during the mission flights. The Falcon aircraft provided a critical capability in DC3 in sampling within the anvil and in close proximity to the storm core.

During the field phase the Falcon aircraft operated over a wide area over the Central U.S., Kansas, Colorado, Wyoming, Nebraska, Missouri, Arkansas, Oklahoma, Texas, and New Mexico, and sampled over 40 flight hours during 13 local flights, as shown in Figure 1. The distant DC3 Alabama area was excluded for Falcon flights. Details on flight planning tools used by the Falcon crew are presented in section 2.3. The main task was to probe the fresh and aged (0–12/12–24 h) anvil outflow from different types of convective systems as supercells, MCCs, MCSs, and squall lines. Furthermore, emissions from wildfires were probed. In general, anthropogenic pollution sources were rather low over the Central U.S. [Barth *et al.*, 2015].

The synoptic situation over the Central U.S. during DC3 was characterized by a number of shortwave troughs propagating from the west to the east, occasionally interacting with the subtropical jet stream. Thunderstorms occurred on a daily basis in different regions over the Central U.S., especially in Texas/Oklahoma and Colorado. In contrast, thunderstorms rarely developed in Kansas and around the operation site except an extended MCS on 30 May [Pan *et al.*, 2014]. A dry line often formed over the Texas Panhandle, where ideal

**Table 1a.** Airborne Falcon Trace Gas Instrumentation Used in the Present Study and in HH2016

Species	Technique	Averaging Time (s)	Horizontal Resolution (km)	Accuracy	Principal Investigator	Reference
Wind ( $u, v, w$ )	Rosemount flow angle sensor	1	~0.2	$1 \text{ m s}^{-1}$ horizontal and $0.3 \text{ m s}^{-1}$ vertical	Andreas Giez, DLR, Germany	Boegel and Baumann [1991]
Temperature	PT100/Rosemount	1		0.5 K		Wendisch and Brenguier [2013]
Humidity	Composite of dewpoint mirror/capacitive sensor/Lyman Alpha absorption instrument	1		5% and 10% below ~5 and 10 km flight altitude, respectively		Wagner et al. [2003]
O <sub>3</sub>	UV absorption	1		±5%	Hans Schlager, DLR, Germany	Baehr et al. [2003]
CO	VUV fluorescence	1		±10%		Gerbig et al. [1999]
NO	NO-O <sub>3</sub> -Chemiluminescence	1		±1 pmol mol <sup>-1</sup>		Ziereis et al. [2000, 2004]
NO <sub>x</sub>	CLD + blue light converter	1		±2 pmol mol <sup>-1</sup>		Pollack et al. [2010]
NO <sub>y</sub>	CLD + NO <sub>y</sub> -Au converter	1		±5 pmol mol <sup>-1</sup>		Ziereis et al. [2000, 2004]
CH <sub>4</sub>	Cavity ringdown analyzer (CRDS)	1		±5%		Chen et al. [2010]
SO <sub>2</sub>	Chemical ionization-ion trap mass spectrometer	10	~2	±20%	Heinfried Aufmhoff, DLR, Germany	Speidel et al. [2007]
VOC	Gas chromatography/flame ionization detector	~1–2 min	~12–24	±15%	Bernhard Rappenglück, University of Houston, USA	Rappenglück et al. [2006] and Leuchner and Rappenglück [2010]

conditions for the initiation of thunderstorms exist: strongly unstable air mass with appreciable vertical wind shear, conditions conducive for supercells. The line separates warm and humid air masses advected from the Gulf of Mexico in the south, from hot and dry air masses advected from the desert regions in the west. The Central U.S. is known to be a preferred region for the development of damaging storms [Schultz et al., 2014].

## 2.2. Falcon Airborne Instrumentation

In the present study we analyze a variety of in situ trace species measurements (CO, O<sub>3</sub>, SO<sub>2</sub>, CH<sub>4</sub>, NO, NO<sub>x</sub>, and rBC) sampled by the Falcon. A similar trace gas instrumentation as described above has been used during several DLR thunderstorm field campaigns in the past [Baehr et al., 2003; Huntrieser et al., 2005, 2007, 2009, 2011]. For details on the aerosol instrumentation see [http://www.pa.op.dlr.de/aerosol/dc3/DLR-IPA\\_AerosolPackage\\_DC3.pdf](http://www.pa.op.dlr.de/aerosol/dc3/DLR-IPA_AerosolPackage_DC3.pdf). The airborne instrumentation used for this study and the accuracies are listed in Tables 1a and 1b. In addition, some trace species (NO<sub>y</sub> and CN) presented first in HH2016 are listed in the overview table. Due to a number of technical problems at the beginning of the DC3 field phase, not all instruments were operational during the first Falcon flights. For example, due to the extremely high temperatures in the flight cabin during the low-level flights in BB plumes, some instruments shut off automatically. In Table 2, a selection of operating instruments for the local Falcon flights is listed. For all instruments in Table 1a (except for SO<sub>2</sub> and VOCs) the averaging time of available data is 1 s. Ozone values are available every 4–5 s, however, interpolated to the 1 s time base of other key trace gases. In Table 1b the averaging time of the aerosol measurements varied between 1 and 10 s depending on the instrument. The resolution of the averaging times is high enough to receive representative measurements during the anvil probing, since the probing of single anvil outflows roughly lasted ~500–2000 s (~100–400 km horizontal extension).

In addition, a video camera was mounted in the Falcon cockpit monitoring the entire flight from start to landing. The videos were partly used to determine the in-cloud time sequences in the anvil outflow and the

**Table 1b.** Airborne Falcon Aerosol Instrumentation Used in the Present Study and in HH2016

Species	Technique	Averaging Time (s)	Horizontal Resolution (km)	Accuracy	Principal Investigator	Reference
Total and nonvolatile CN concentration	Condensation particle counter with/without thermal denuder	1	~0.2	±10%	Andreas Minikin, DLR, Germany	Minikin et al. [2012]
Cloud particle number concentration and size (2–50 $\mu\text{m}$ )	Optical scattering (FSSP-100)	5	~1	±25%	Andreas Minikin, DLR, Germany	Minikin et al. [2012]
Refractory black carbon mass	Single particle soot photometer (SP2)	10	~2	±20%	Bernadett Weinzierl, DLR, Germany	Laborde et al. [2012] and Dahlkötter et al. [2014]

**Table 2.** Available Falcon Measurements During DC3 (Only Selected Trace Species From Tables 1a and 1b Are Considered)

DC3 Flight Number, Date, Flight a or b	CO	O <sub>3</sub>	SO <sub>2</sub>	CH <sub>4</sub>	NO	NO <sub>x</sub>	NO <sub>y</sub>	VOC	rBC
F#1 290512a	-	x	-	-	-	-	-	x	x
F#2 290512b	-	x	x	-	-	-	-	x	-
F#3 300512a	x	x	x	-	x	-	-	x	x
F#4 300512b	x	x	x	-	x	-	-	x	x
F#5 050612a	x	x	x	x	x	x	-	x	x
F#6 050612b	x	x	x	x	x	x	-	x	x
F#7 060612a	x	x	x	x	-	-	-	x	x
F#8 080612a	x	x	x	x	x	-	x	x	x
F#9 080612b	x	x	x	x	x	-	x	x	x
F#10 110612a	x	x	x	x	x	x	-	x	x
F#11 110612b	x	x	x	x	x	x	-	x	x
F#12 120612a	x	x	x	x	x	x	-	x	x
F#13 140612a	x	x	x	x	x	x	-	x	x

presence of smoke from wildfires. Further, the Falcon was equipped with a standard meteorological measurement system to measure position, altitude, temperature, pressure, humidity, and the three-dimensional wind vector ( $u, v, w$ ). All flight altitude values refer to pressure height and UTC (universal time coordinated) time. The time difference between UTC and the central daylight time (CDT) in Salina is +5 h (e.g., 06:00 CDT = 11:00 UTC).

During DC3, the performance of similar instruments on different aircraft was tested during several intercomparison flights [Pollack *et al.*, 2016]. The Falcon aircraft performed an intercomparison flight with the DC8 on 11 June 2012 in polluted (BB) and clean air masses. At the first level of the intercomparison (2.1 km) at 16:30–16:50 UTC the Falcon and DC8 aircraft measured similar mean O<sub>3</sub> mixing ratios:  $59 \pm 1$  and  $60 \pm 1 \text{ nmol mol}^{-1}$ , respectively. The mean CO mixing ratios measured by the Falcon were slightly higher compared to the DC8:  $142 \pm 9$  and  $139 \pm 10 \text{ nmol mol}^{-1}$ , respectively. At the second level of the intercomparison (6.4 km) at 17:02–17:15 UTC mean O<sub>3</sub> mixing ratios agreed well for both aircraft ( $47 \pm 3 \text{ nmol mol}^{-1}$ ), whereas the mean CO mixing ratios measured by the Falcon ( $83 \pm 6 \text{ nmol mol}^{-1}$ ) were again slightly higher than measured by the DC8 ( $81 \pm 6 \text{ nmol mol}^{-1}$ ). Overall, CO and O<sub>3</sub> mixing ratios between the Falcon and DC8 agreed well (less than 2% difference). For NO, mean mixing ratios measured by the Falcon were distinctly higher than measured by the DC8: at the first level 126 compared to  $39 \text{ pmol mol}^{-1}$  and at the second level 145 compared to  $23 \text{ pmol mol}^{-1}$  (the lower values are close to the detection limit). Unfortunately, the Falcon NO instrument was not working properly during the intercomparison performed soon after the takeoff (16:11 UTC). The flight cabin was still too hot which caused a very unstable zero point. The limit of detection for NO was distinctly higher ( $\sim 50 \text{ pmol mol}^{-1}$ ) than during the other Falcon DC3 flights ( $\sim 20 \text{ pmol mol}^{-1}$ ). In addition, the highly unstable zero point during this flight due to the heat caused an uncertainty of  $\pm 50 \text{ pmol mol}^{-1}$ , which may explain the differences in the NO measurements during the intercomparison.

Unfortunately, no direct intercomparisons between NO<sub>2</sub> and NO<sub>x</sub> from the Falcon and DC8 are available. However, to achieve some information on the general performance of the instruments, we compared the mean NO background values given later in section 3.2 for the Falcon, DC8, and GV aircraft. Here we estimate that in the free tropospheric background air at  $\sim 2\text{--}8$  km altitude, the Falcon NO measurements are on average higher by  $\sim 0.06$  and  $\sim 0.05 \text{ nmol mol}^{-1}$  NO, respectively, than both the DC8 ( $0.03 \text{ nmol mol}^{-1}$ ) and GV ( $0.04 \text{ nmol mol}^{-1}$ ) background measurements, most likely due to the higher detection limit of the Falcon instrument. For the flight on 11 June, we also compared the NO<sub>x</sub> measurements of the Falcon and the NO and NO<sub>2</sub> (NO + NO<sub>2</sub>  $\approx$  NO<sub>x</sub>) measurements of the DC8 when the aircraft were flying in the free tropospheric background ( $\sim 2\text{--}8$  km). The average Falcon NO<sub>x</sub> mixing ratios were in the range of  $0.30 \text{ nmol mol}^{-1}$ , while the DC8 measurements indicated average NO<sub>x</sub> mixing ratios in the range of  $0.13 \text{ nmol mol}^{-1}$  for the free tropospheric background.

On several days (25 and 30 May and 1, 5, and 17 June) also intercomparison flights between the NASA-DC8 and NSF/NCAR-GV aircraft were performed. The average percent differences between these two aircraft were in the range of 2% for NO, 28% for NO<sub>2</sub>, 5% for CO, and  $<1\%$  for O<sub>3</sub> [Pollack *et al.*, 2016]. The large difference

in the NO<sub>2</sub> measurements may result from the thermal dissociation of methylperoxynitrate applied to DC8 NO<sub>2</sub> instrument [Nault *et al.*, 2015]. A total uncertainty of 30% for NO<sub>x</sub> measured in storms sampled by the GV and DC8 and an overall uncertainty of 55% for NO<sub>x</sub> measured in storms sampled by the Falcon were applied by Pollack *et al.* [2016].

### 2.3. Flight Planning Tools and Postanalysis Products

For the flight planning support and postanalysis of the Falcon in situ data, a variety of meteorological products are available from the DC3 field catalog (<http://catalog.eol.ucar.edu/dc3/>).

Experimental products, e.g., the high-resolution rapid refresh forecasts by NOAA showing the composite reflectivity for the Central U.S. on an hourly basis (<http://ruc.noaa.gov/hrrr/>), were successfully applied by the Falcon team to predict favored regions of thunderstorm development within the DC3 domains (not shown). This data product is based on an hourly updated cloud-resolving atmospheric model, initialized by 3 km grids with 3 km radar assimilation over a 1 h period.

The general cloud development over the DC3 operation area was analyzed by using different kinds of visible/VIS (channel 1) and infrared/IR (channel 4) products with a high temporal (5–10 min) and spatial resolution (1–4 km) from the Geostationary Environmental Operational Satellite 13, i.e., cloud top heights derived from the thermal-IR cloud top temperatures (available from the DC3 data catalog, <http://catalog.eol.ucar.edu/dc3/>). Furthermore, GOES East–Aerosol/Smoke Products (GASP) available every 30 min were used for the monitoring of extensive smoke plumes, as frequently observed during DC3. The GASP product is a retrieval of the aerosol optical depth (AOD) made from the current GOES East visible imagery (<http://www.ssd.noaa.gov/PS/FIRE/GASP/>). This product is available at a 4 km × 4 km spatial resolution during the sunlit portion of the day. Natural color images from the Moderate Resolution Imaging Spectroradiometer (MODIS) (<http://modis.gsfc.nasa.gov/>) on NASA's Aqua satellite (<http://aqua.nasa.gov/>) were used to retrieve the position of active wildfires and the spreading of the smoke plumes.

Optical measurements from the NASA Langley Airborne Differential Absorption Lidar-High Spectral Resolution Lidar system on board the DC8 aircraft were used in the present study to analyze 2-D vertical cross sections of ozone concentration and particulate backscatter, extinction, and depolarization near thunderstorms. The system incorporates multiple lasers to produce five different wavelengths that are transmitted in the zenith and nadir direction. Two wavelengths (292 and 300 nm) are used to measure ozone [Browell, 1989]. The instrument also incorporates backscatter, extinction, and depolarization measurements at 532 nm via the high spectral resolution lidar technique and backscatter and depolarization at 355 and 1064 nm using standard lidar retrievals [Hair *et al.*, 2008]. Uncertainties in the ozone and aerosol profiles are assessed during each campaign and have previously been compared to state-of-the-art in situ and remote sensing measurements [e.g., Rogers *et al.*, 2009].

For the monitoring of the flight track during the field missions, the NCAR Earth Observing Laboratory (EOL) operation tool was successfully used. The GOES 13 satellite images were overlaid by constant altitude plan position indicator images from the Next-Generation Radar (NEXRAD): a network of 160 high-resolution S-band Doppler weather radars operated by the National Weather Service (<http://www.roc.noaa.gov/WSR88D/>). Furthermore, the NCAR-EOL operation tool offered the possibility to overlay lightning data from the National Lightning Detection Network (NLDN) and flight track data on the satellite images. The NLDN system is operated by the Vaisala Thunderstorm Unit [Cummins and Murphy, 2009] (<http://thunderstorm.vaisala.com/>). Based on the information from this NCAR-EOL operation tool, the ground crew sometimes contacted the pilots (by satellite phone), e.g., to redirect the heading of the aircraft to avoid areas with a high lightning frequency not visible to the pilots on the aircraft radar. Similar images as the NCAR-EOL operation tool images are shown in the present study; however, in addition, O<sub>3</sub> distributions along the flight track have been superimposed.

Detailed radar measurements were performed from the ground in Oklahoma/Texas with the Shared Mobile Atmospheric Research and Teaching (SMART) single and dual polarized C-band Doppler radars (SR1 and SR2) [Biggerstaff *et al.*, 2005]. Multi-Doppler 3DVAR analyses of SMART radar data were used to derive the vertical velocity within the storms. The analysis technique follows Potvin *et al.* [2012].

Online Hybrid Single-Particle Lagrangian Integrated Trajectory (HYSPLIT) backward trajectories [Draxler and Rolph, 2014; Rolph, 2014] (<http://ready.arl.noaa.gov/HYSPLIT.php>) were used to determine the age of emissions from wildfires probed by the Falcon aircraft. The trajectory calculations were run with North

American Mesoscale data from National Centers for Environmental Prediction (NCEP) with a horizontal resolution of 12 km.

A 10 year climatology (2005–2014) of Aura MLS version 3 data products [Livesey *et al.*, 2011; Schwartz *et al.*, 2013] was used to analyze the occurrence of elevated H<sub>2</sub>O at 100 hPa (~16 km) over the U.S. and globally during the months May–June (spatial resolution: 3 km in the vertical and 200 km along the orbital-track line). The global grid has 78 longitudinal bins (~4.6° spacing) and 30 latitudinal bins (~6° spacing), with the bin edges chosen to have a uniform number of MLS observations per bin (~900 for May–June for the mission), and for them to be symmetrically located within the bins, based upon the known 16 day orbital repeat cycle. Bin statistics are mean and maximum of all observations within a bin that pass screening. The uncertainty of MLS H<sub>2</sub>O data at 100 hPa is about 10% [Read *et al.*, 2007].

### 3. Falcon Observations During DC3

A general overview of the Falcon observations is given next. In section 3.1 the influence from *wildfires* is presented on the basis of vertical profiles of trace species (CO, SO<sub>2</sub>, CH<sub>4</sub>, O<sub>3</sub>, and rBC). In section 3.2 vertical profiles of NO and NO<sub>x</sub> are analyzed focusing on *lightning-produced NO<sub>x</sub>* and compared to profiles from past thunderstorm field experiments.

#### 3.1. Influence From Wildfires

Mean vertical profiles of trace species (CO, SO<sub>2</sub>, CH<sub>4</sub>, O<sub>3</sub>, and rBC) are shown in Figures 2a–2e in different colors for every single Falcon flight. Mean values for every 250 m altitude bin are given. For every species the white profiles show average profiles for the entire DC3 campaign. Except for O<sub>3</sub> (stratospheric source), all vertical profiles show a general decrease with altitude. Besides the common enhancements in the BL due to surface pollution, it is obvious that strongly polluted layers (especially enhanced in CO, SO<sub>2</sub>, and rBC) were observed during numerous flights throughout the entire troposphere up to ~10 km. These lofted pollution layers (BB plumes) originated from strong wildfires as described next.

During the DC3 field experiment, some of the largest and most destructive wildfires in New Mexico (NM) and Colorado state's history were burning: the Whitewater-Baldy (NM), the Little Bear (NM), and the High Park Fire in Colorado. See Table 3 and Lang *et al.* [2014] for more details. All of these fires were initiated by lightning. On 9 June 2012 extended smoke plumes from the NM fires were advected northeastward into the DC3 domain, as shown in the MODIS and GOES-AOD images in Figures 3a and 3b. These fire emissions frequently accumulated along the border to Texas and over the Texas Panhandle, where the dry line acts as a barrier between dry and humid air masses. Apart from anthropogenic pollution surrounding larger cities, the general pollution influence during DC3 mainly originated from these wildfires. Occasionally, smaller wildfires were active that partly impacted the DC3 flights but are not listed in Table 3, e.g., the Little Sand Fire in southern Colorado ([http://en.wikipedia.org/wiki/2012\\_Colorado\\_wildfires](http://en.wikipedia.org/wiki/2012_Colorado_wildfires)) and the Hewlett Gulch Fire near Fort Collins in northern Colorado [Lang *et al.*, 2014].

The most suitable tracers measured by the Falcon for identifying upward transport of pollution (of biomass and anthropogenic origin) from the BL to the UT were CO and CH<sub>4</sub> with lifetimes on the order of ~2–3 months and ~9 years in the troposphere, respectively [e.g., Xiao *et al.*, 2007]. In contrast, SO<sub>2</sub> and rBC were useful tracers in some cases when BB plumes were advected to the lower and mid troposphere. However, during convective uplift to the UT these trace species were frequently washed out by precipitation. While CO and rBC are well-known trace species emitted by wildfires, SO<sub>2</sub> is less known. The sulfur in wildfire emissions originates from amino acids present in the vegetation. Independently, ozone can partly be used as a tracer for upward transport due to its general increase with altitude throughout the troposphere (BL excluded). Ozone has a lifetime in the range of days to months [Arlander *et al.*, 1995; Stevenson *et al.*, 2006].

In contrast to the rather straight average DC3 CO profile (except BL), the average CH<sub>4</sub> profile (Figure 2c, white line) had a more pronounced shape, with mixing ratios in the range of 1900 nmol mol<sup>-1</sup> in the BL and decreasing mixing ratios in the mid troposphere down to 1830 nmol mol<sup>-1</sup>. At ~10–11 km, mean CH<sub>4</sub> mixing ratios were slightly enhanced up to 1850 nmol mol<sup>-1</sup>, most likely due to uplift of pollution from the BL by deep convection; see section 3.2. The vertical profiles for O<sub>3</sub> showed rather constant values in the lower and mid troposphere on average in the range of 60–70 nmol mol<sup>-1</sup> without any distinct influence from lofted

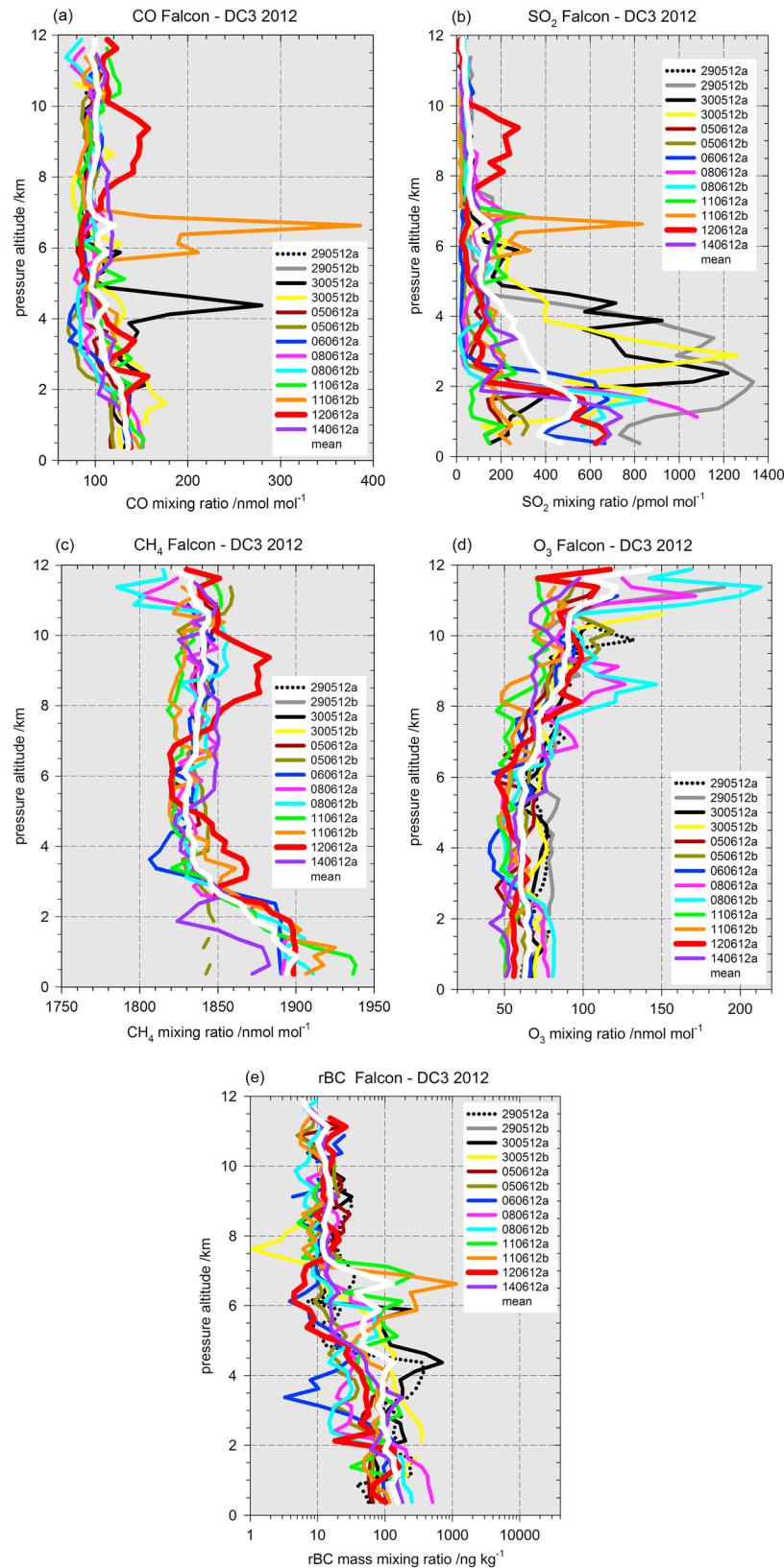


**Figure 2.** Mean vertical profiles for (a) CO, (b) SO<sub>2</sub>, (c) CH<sub>4</sub>, (d) O<sub>3</sub>, and (e) rBC derived from measurements with the Falcon aircraft. Mean values for every 250 m altitude bin are given for available DC3 flights in different colors according to date (ddmmyy). The mean vertical profile of all colored flight profiles in each figure is indicated as a white line.

**Table 3.** Active Wildfires Impacting the Falcon Flights (Partly Adapted From [http://en.wikipedia.org/wiki/List\\_of\\_wildfires](http://en.wikipedia.org/wiki/List_of_wildfires) and [http://en.wikipedia.org/wiki/List\\_of\\_Colorado\\_wildfires](http://en.wikipedia.org/wiki/List_of_Colorado_wildfires) Updated in February 2015)

Date of Fire Start	Region	Name (Latitude/Longitude)	Area Burned	Initiation	Comments
9/16 May 2012	New Mexico (SW) (Gila National Forest)	Whitewater-Baldy (33°N/108°W)	289,478 acres (117,148 ha)	Lightning	Baldy and Whitewater fires merged on 23 May. By 29 May, <i>largest wildfire in New Mexico state history</i> .
4 June 2012	New Mexico (S) (Lincoln National Forest)	Little Bear (33°N/106°W)	44,330 acres (17,940 ha)	Lightning	By 11 June, the fast burning fire had destroyed ~35,000 acres. <i>Most destructive wildfire in New Mexico state history</i> .
9 June 2012	Colorado (N) (near Fort Collins)	High Park (41°N/105°W)	87,284 acres (35,323 ha)	Lightning	By 12 June, the fire had burned ~43,000 acres. <i>Third largest wildfire by size and third most destructive wildfire in Colorado state history</i> .

BB plumes (Figure 2d). In the UT, a general increase of O<sub>3</sub> mixing ratios with height is visible, due to the proximity to the O<sub>3</sub>-rich stratosphere. The lofted BB plumes were not pronounced in the vertical NO and NO<sub>x</sub> profiles shown in Figures 4a and 4b, mainly due to the short lifetime of NO<sub>x</sub> in the BL and LT (only a few hours).

Compared to the distinct presence of lofted BB plumes during many DC3 flights, the influence from anthropogenic BL emissions was not very pronounced in the vertical profiles. During takeoff and landing over Salina (KS), Lubbock (TX), Ardmore (OK), Wichita Falls (TX), and Oklahoma City (OK), the average CO mixing ratios in the BL were in the range of 130–140 nmol mol<sup>-1</sup> (partly also enhanced from aged BB emissions) and only slightly enhanced compared to ~100–110 nmol mol<sup>-1</sup> in the lower and mid troposphere background (Figure 2a). On the other hand, SO<sub>2</sub> and rBC mixing ratios were distinctly more elevated in the lofted BB plumes compared to the BL in general (Figures 2b and 2e).

During DC3, the most pronounced BB plumes (Figures 2a, 2b, and 2e) were observed on 29–30 May and 11–12 June 2012. Plume criteria and further plume details are listed in Table 4 such as fire source, distance from source, plume height and age, and trace species mixing ratios. The source region and age of the selected BB plumes were determined by online HYSPLIT backward trajectory calculations (here) and partly by particle dispersion model simulations (FLEXPART; see HH2016). The BB plumes were probed ~600–1000 km downstream from the fire sources, and the plume age varied between ~9 and 27 h.

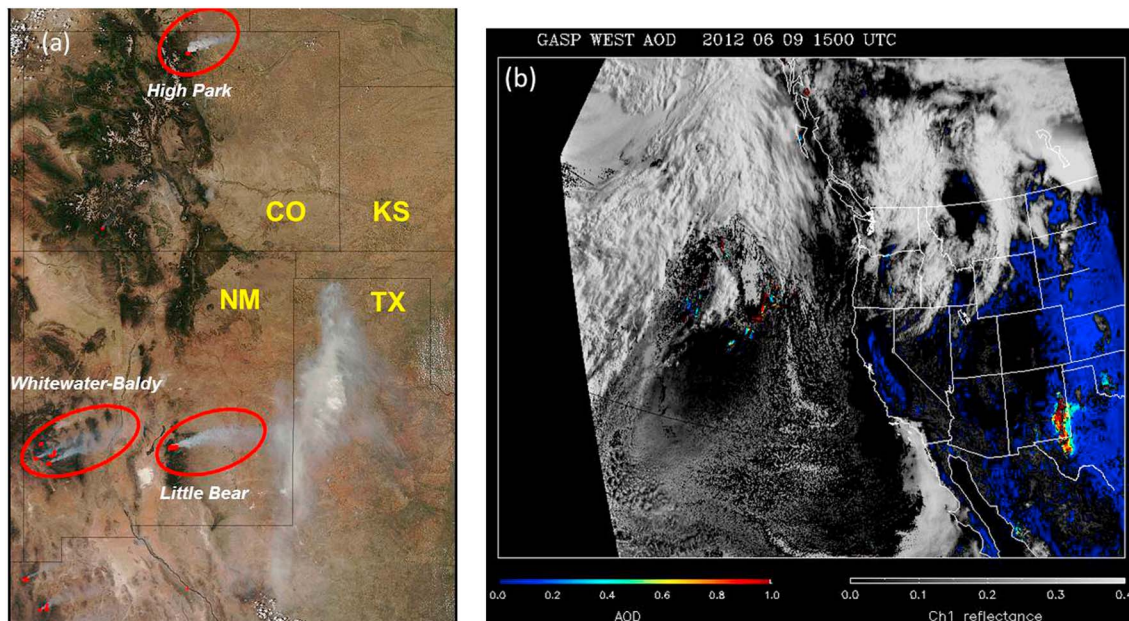


**Figure 3.** (a) MODIS image from 9 June 2012 at 19:45 UTC. The positions of actively burning fires are marked with red dots. The red circles mark the smoke plumes from the High Park, Whitewater-Baldy, and Little Bear wildfires. (b) Aged smoke plumes from the New Mexican fires accumulated eastward along the border to Texas as also visible in the GOES aerosol optical depth (AOD) image from 9 June 2012 at 15:00 UTC.

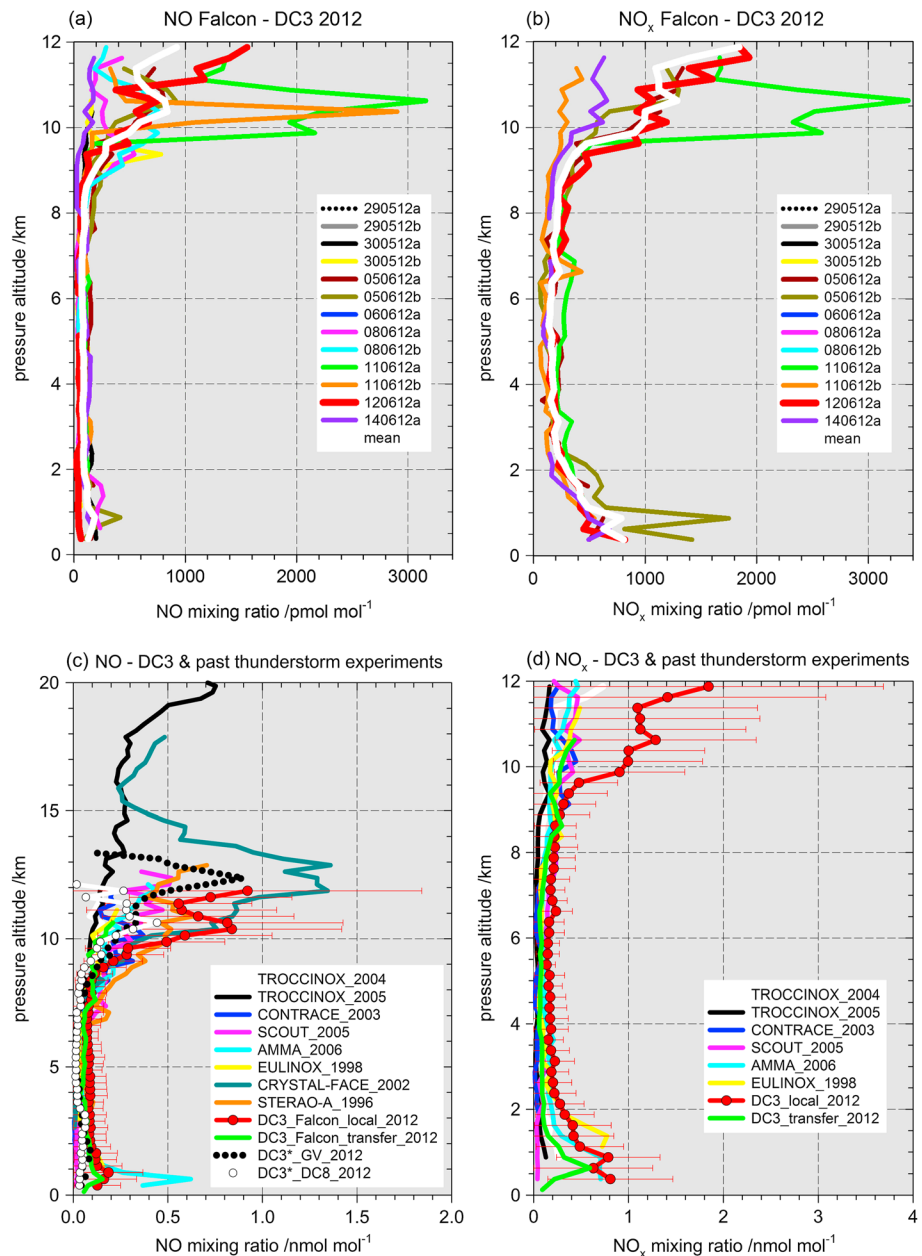


**Figure 4.** Mean vertical profiles for (a, c) NO and (b, d) NO<sub>x</sub> during DC3 and past airborne thunderstorm experiments (see text). Mean values for every 250 m altitude bin are given in different colors according to the DC3 flight date (ddmmmyy) or field campaign. The mean vertical profile of all colored DC3 flight profiles in Figures 4a and 4b is indicated as a white line. DC3\* in Figures 4c and 4d includes only the DC8 and GV flights on 29 and 30 May and 5, 6, and 11 June 2012.

Biomass burning emissions were observed at all altitudes in the troposphere: the Whitewater-Baldy Fire plume in the BL and up to ~6 km, the Little Bear Fire plume at ~6–7 km, and the High Park Fire plume at ~7–10 km. The uplift of BB plumes to the UT will be discussed in section 5. Most of the dense BB plumes were probed in the vicinity of thunderstorms and visible to the aircraft crew by their brownish color. Occasionally, these BB emissions were ingested into/nearby thunderstorms and observed within or just below the anvil outflow region as discussed in section 5.

Emissions from the New Mexican Whitewater-Baldy Fire strongly impacted the first Falcon flights on 29–30 May, whereas emissions from the Little Bear Fire were the main contributor to the extremely polluted layers observed on 11 June. Later during the campaign, wildfires in Colorado (High Park) were pronounced sources

**Table 4.** Most Intense Biomass Burning (BB) Plumes Probed by the Falcon ( $\triangleq$  the Six Strongest Plumes in the Free Troposphere With Mean CO  $> 120 \text{ nmol mol}^{-1}$  and SO<sub>2</sub>  $> 200 \text{ pmol mol}^{-1}$  or rBC  $> 200 \text{ ng kg}^{-1}$  Selected From Figures 2a, 2b, and 2e)

DC3 Flight Number, Date, Flight a or b	Flight UTC (s)	Flight Position (Latitude/Longitude)	Fire Source (Latitude/Longitude)	Distance From Fire Source (km)	BB Plume Height (Depth) (km)	BB Plume Age (h)	Mean (Maximum) CO (nmol mol $^{-1}$ )	Mean (Maximum) SO <sub>2</sub> (pmol mol $^{-1}$ )	Mean NO (NO <sub>x</sub> ) (nmol mol $^{-1}$ )	Mean (Maximum) rBC Mass Mixing Ratio (ng kg $^{-1}$ )
F#1 290512a	77,621–77,981	33°N/100°W	Whitewater-Baldy (33°N/108°W)	~800	1.0–4.2 (3.2)	~21–27	—	—	—	419 (1,477)
F#2 290512b	84,226–84,473	34°N/102°W	Whitewater-Baldy (33°N/108°W)	~600	1.0–4.6 (3.6)	~12–24	—	—	1431 (2,587)	—
F#3 300512a	73,736–74,133	34°N/102°W	Whitewater-Baldy (33°N/108°W)	~600	<2.2–5.2 (>3.0)	~12–24	268 (472)	970 (2,920)	0.14 (–)	571 (1,295)
F#4 300512b	91,143–91,669	34°N/102°W	Whitewater-Baldy (33°N/108°W)	~600	1.0–5.6 (4.6)	~12–24	163 (203)	815 (3,870)	0.05 (–)	213 (365)
F#11 110612b	73,803–74,467	36°N/98°W	Little Bear (33°N/106°W)	~1,000	5.7–6.9 (1.2)	~24–27	380 (721)	767 (1,642)	0.12 (0.36)	874 (1,643)
F#12 120612a	(gap 73,964–74,075) 88,029–88,372	39°N/99°W	High Park (41°N/105°W)	~600	7.0–9.7 (2.7)	~9	143 (178)	200 (504)	0.08 (0.31)	16 (41)

of BB emissions, which impacted the Falcon flight on 12 June. In section 5 in the present study we focus more in detail on the 29 May case. The flights from 30 May and 12 June are described in more detail in HH2016.

The most pronounced BB plume was observed northeast of Oklahoma City during the second flight on 11 June (b flight). As far distant as  $\sim 1000$  km from the Little Bear Fire, elevated CO mixing ratios exceeding  $700 \text{ nmol mol}^{-1}$  (mean  $380 \text{ nmol mol}^{-1}$ ) were measured at  $\sim 6\text{--}7$  km altitude (Table 4 and Figure 2a). Furthermore, peak SO<sub>2</sub> and rBC mixing ratios reached up to  $\sim 1600 \text{ pmol mol}^{-1}$  and  $\sim 1600 \text{ ng kg}^{-1}$ , respectively. The plumes probed on 29–30 May were located near Lubbock,  $\sim 600\text{--}800$  km downstream from the Whitewater-Baldy Fire. Mean CO and SO<sub>2</sub> mixing ratios in the layer  $\sim 1\text{--}6$  km varied between  $\sim 160\text{--}270 \text{ nmol mol}^{-1}$  and  $\sim 800\text{--}1400 \text{ pmol mol}^{-1}$ , respectively. The mean rBC mass mixing ratios varied between  $\sim 200$  and  $600 \text{ ng kg}^{-1}$ . The most elevated plume ( $\sim 7\text{--}10$  km) was probed on 12 June just west of Salina about  $\sim 600$  km from the High Park Fire. Mean CO and SO<sub>2</sub> mixing ratios were slightly enhanced:  $\sim 140 \text{ nmol mol}^{-1}$  and  $200 \text{ pmol mol}^{-1}$ , respectively. In contrast, the mean rBC mass mixing ratio was low ( $16 \text{ ng kg}^{-1}$ ) most likely due to processing in deep convection.

In all BB plumes listed in Table 4, NO and NO<sub>x</sub> mixing ratios were low ( $\sim 0.1$  and  $\sim 0.3 \text{ nmol mol}^{-1}$ , respectively) and close to typical background values. The ozone mixing ratio in the BB plumes located at  $\sim 1\text{--}7$  km mainly varied between  $\sim 70$  and  $80 \text{ nmol mol}^{-1}$ , which is roughly  $\sim 10 \text{ nmol mol}^{-1}$  more than in the typical background (Figure 2d) indicating O<sub>3</sub> production. More details on O<sub>3</sub> in BB plumes and its correlation with CO are discussed separately in HH2016.

### 3.2. Influence From LNO<sub>x</sub>

While emissions from wildfires were especially pronounced in the lower and midparts of the vertical CO, SO<sub>2</sub>, and rBC profiles ( $< 10$  km), nitrogen oxide emissions produced by lightning dominated the uppermost layers of the vertical NO and NO<sub>x</sub> profiles at  $\sim 9\text{--}12$  km, as shown in Figures 4a and 4b (mean values for every 250 m altitude bin are given). Detailed lightning distributions for selected flights with elevated UT-NO<sub>x</sub> are presented in HH2016. The highest NO peaks measured by the Falcon were in a supercell over northern Texas on 30 May 2012 with values up to  $9 \text{ nmol mol}^{-1}$  at 9 km altitude (1 s values; see section 4.1). The highest mean NO and NO<sub>x</sub> mixing ratios averaged over the anvil outflow region,  $\sim 3 \text{ nmol mol}^{-1}$ , were observed during a flight on 11 June (green line in Figures 4a and 4b) in a MCS over Missouri and Arkansas (outflow altitude 9.5–11.0 km). The GV aircraft measured peak NO<sub>x</sub> mixing

ratios as high as 15–16 nmol mol<sup>-1</sup> in the same system. The Falcon mean NO and NO<sub>x</sub> mixing ratios are in the same range as observed in the Hector thunderstorm system in Darwin, Australia, during SCOUT-O3 [Huntrieser *et al.*, 2009], which is counted among the storms with the highest LNO<sub>x</sub> production worldwide.

During DC3, the primary tropopause in the Falcon operation area was located at ~11–12 km; however, a previous analysis indicates that the tropopause transition zone in this region can frequently reach up to 14–15 km (O. Cooper, Analysis of radiosonde data, personal communication, 2012). The top of the anvil outflow was frequently located above the maximum cruising altitude of the Falcon (12.4 km). On 12 June, continuously increasing NO and NO<sub>x</sub> mixing ratios with altitude indicate that the top of the anvil outflow from a squall line over Kansas was most likely located above 12 km and not reachable by the aircraft (red line in Figures 4a and 4b). The slight “C” shape of the mean vertical NO<sub>x</sub> profile (Figure 4b, white line), with a maximum of ~2 nmol mol<sup>-1</sup> in the UT, shows that LNO<sub>x</sub> clearly exceeded the pollution sources in the BL on average (<1 nmol mol<sup>-1</sup>), as will be discussed in more detail in section 4.1.

In Figures 4c and 4d mean NO and NO<sub>x</sub> vertical profiles from DC3 (all Falcon profiles, selected DC8 and GV profiles) are compared to vertical profiles obtained from past airborne thunderstorm experiments performed over the Central and southeastern U.S., e.g., STERAO-A and CRYSTAL-FACE [Dye *et al.*, 2000; Ridley *et al.*, 2004], and over other continents (Europe: EULINOX, CONTRACE; South America: TROCCINOX; Africa: AMMA; Australia: SCOUT-O3) [Huntrieser *et al.*, 2002, 2005, 2007, 2008, 2009, 2011; Schumann and Huntrieser, 2007]. For the GV and DC8 aircraft only vertical profiles from the DC3 time period 29 May to 14 June 2012 were considered when the Falcon operated from Salina. In Figure 4c the y axis reaches up to 20 km since data from two high-flying aircraft were included. The results clearly show that average NO and NO<sub>x</sub> mixing ratios in the UT/LS region were generally higher during DC3 than observed during most previous thunderstorm experiments, except for CRYSTAL-FACE in Florida where a “faucet” of NO is known to be produced by lightning [Ridley *et al.*, 2004]. In addition, measurements from another U.S. field campaign, STERAO-A in Colorado [Dye *et al.*, 2000], also show enhanced NO mixing ratios in a similar range as observed during DC3 at these altitudes. Interestingly, the vertical NO distributions for STERAO-A and DC3 show two distinct maxima in the UT/LS region, a primary one at ~10–11 km and a secondary one at ~12–13 km. The primary (secondary) one is generally located in the UT, just below (above) the main tropopause at ~11–12 km. As discussed in HH2016, a double-tropopause structure was frequently observed in the region of the subtropical jet stream. Poleward Rossby wave breaking has been suggested to cause these large-scale double-tropopause events [Homeyer *et al.*, 2014]. Such a setting promotes the development of overshooting tops and the detrainment of anvil-NO into the LMS, as will be discussed in section 4.1. Measurements in the subtropics during CRYSTAL-FACE show that anvil-NO spread over a wide altitude range ~10–15 km, with a maximum at ~12–13 km (Figure 4c). This maximum coincides with the secondary maximum observed during DC3 and STERAO-A and suggests that these thunderstorms developed along the subtropical jet stream in a transition zone between the lower extratropical and the higher subtropical tropopause.

In summary, thunderstorm measurements performed over the Central and southeastern U.S. showed especially high NO and NO<sub>x</sub> mixing ratios in the UT/LS region (~9–12 km) compared to past Falcon thunderstorm experiments carried out over other continents. This result is in agreement with general results on strong thunderstorm activity over the Central and southeastern U.S. as presented in section 1. In addition, we suggest that the frequent probing and the wide horizontal spreading of the anvil outflow during DC3 contributed to enhance average NO and NO<sub>x</sub> mixing ratios in the UT/LS region compared to other thunderstorm campaigns shown in Figures 4c and 4d. In the next subsection tracer-tracer analyses are conducted to show that LNO<sub>x</sub> was the dominating NO<sub>x</sub> source in the UT/LS region during DC3.

## 4. Evidence of Convective Injection Into the Lowermost Stratosphere

### 4.1. LNO<sub>x</sub> in the UT/LS Region and Its Correlation With CO and O<sub>3</sub>

The sources of nitrogen oxides measured in the anvil outflow are twofold. In addition to LNO<sub>x</sub>, NO<sub>x</sub>-rich air from the polluted BL may be transported upward by the thunderstorm and contributes to enhanced NO<sub>x</sub> mixing ratios in the anvil outflow region. The vertical profiles in Figure 4b showed that NO<sub>x</sub> mixing ratios in the BL (thunderstorm inflow region) were, in general, lower than in the thunderstorm outflow region (~9–12 km). This finding indicates that the anvil outflow of DC3 thunderstorms was most likely dominated

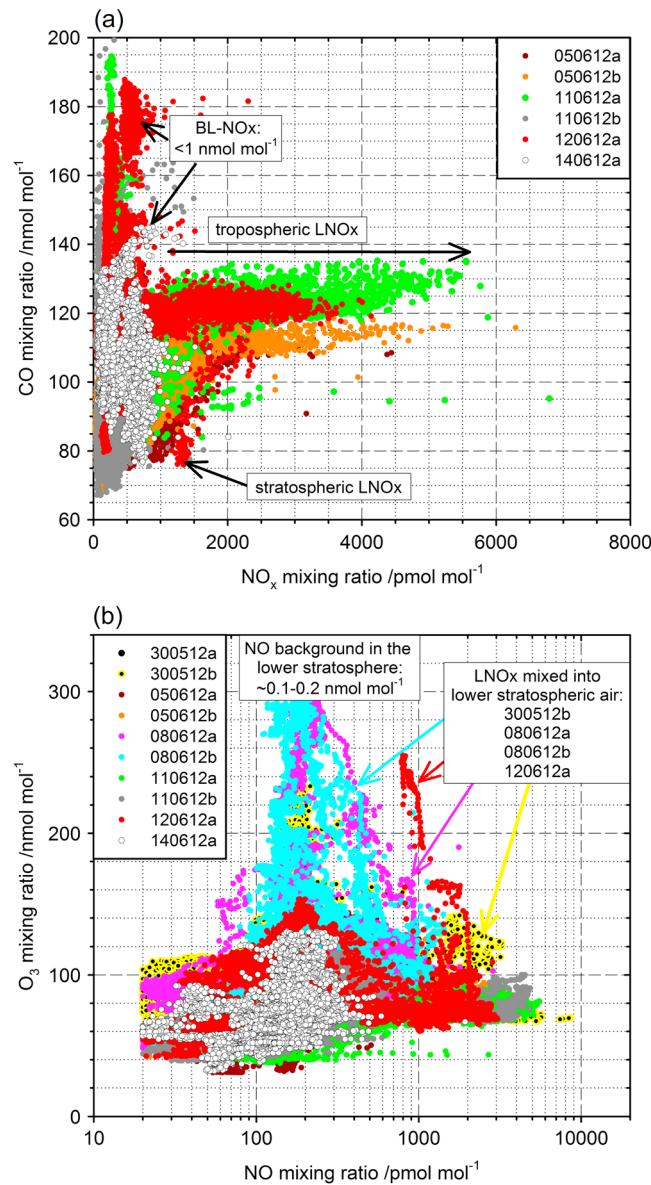


**Figure 5.** (a) CO-NO<sub>x</sub> correlations for all DC3 Falcon flights with available NO<sub>x</sub> measurements. (b) O<sub>3</sub>-NO correlations for all DC3 Falcon flights with available NO measurements (color coded according to date; ddmmmyy).

by LNO<sub>x</sub> and the contribution from BL-NO<sub>x</sub> was only minor, which is in agreement with Pollack *et al.* [2016]. A similar finding was made by DeCaria *et al.* [2000, 2005] for a STERAO-A storm over Colorado. More informative tracer-tracer correlations are presented next to confirm this finding.

For all available DC3 Falcon flights (Table 2), the correlation between NO<sub>x</sub> and CO, and NO and O<sub>3</sub>, is used to compare the amount of LNO<sub>x</sub> to background-NO<sub>x</sub> in the BL (takeoff and landing) and UT/LS (anvil outflow region). Based on this data set, the highest NO<sub>x</sub> mixing ratios ( $\sim 7 \text{ nmol mol}^{-1}$ ) were observed on 11 June in a MCS probed along the border between Oklahoma, Missouri, and Arkansas, as shown in Figure 5a. Thunderstorms were also investigated on 5 and 12 June, as visible in the pronounced NO<sub>x</sub> enhancements. In contrast, no active thunderstorms were probed on 14 June. The latter measurements and the measurements in the BL show that background-NO<sub>x</sub> mixing ratios were generally low ( $<1 \text{ nmol mol}^{-1}$ ). Within the anvil outflow, NO<sub>x</sub> produced by lightning within the range  $\sim 1\text{--}7 \text{ nmol mol}^{-1}$  was distinctly enhanced compared to the background and BL. In addition, CO mixing ratios were enhanced in the outflow,  $\sim 105\text{--}135 \text{ nmol mol}^{-1}$ , indicating upward transport of polluted air masses from the BL by deep convection. The injection of LNO<sub>x</sub> into the lowermost stratosphere was especially pronounced on 12 June, where enhanced NO<sub>x</sub> mixing ratios in the range of  $1.5 \text{ nmol mol}^{-1}$  coincided with very low CO mixing ratios ( $<80 \text{ nmol mol}^{-1}$ ).

The injection of LNO<sub>x</sub> into lower stratospheric air masses is even better visible in Figure 5b, where O<sub>3</sub>-NO correlations for all available Falcon flights are shown. Measurements on 8 June partly indicate that NO background mixing ratios in the lowermost stratosphere ( $O_3 > 150 \text{ nmol mol}^{-1}$ ) are low and in the range of  $\sim 0.1\text{--}0.2 \text{ nmol mol}^{-1}$  (background mixing ratios in agreement with Ziereis *et al.* [2000]). In contrast, a mixture of LNO<sub>x</sub> with lower stratospheric air masses is clearly visible on 30 May (b flight), 8 June (a + b flight), and 12 June (flights discussed in detail in HH2016). Here elevated NO mixing ratios ( $\sim 0.3\text{--}3 \text{ nmol mol}^{-1}$ ) coincide with elevated O<sub>3</sub> mixing ratios ( $\sim 100\text{--}260 \text{ nmol mol}^{-1}$ ). These correlations clearly stand out compared to the general O<sub>3</sub>-NO correlation pattern for the troposphere and lowermost stratosphere given by the rest of the Falcon flights.

In summary, the Falcon observations during DC3 indicate that thunderstorms strongly impact the NO and NO<sub>x</sub> budget in the UT/LS region over the Central United States. During four flights a pronounced mix of

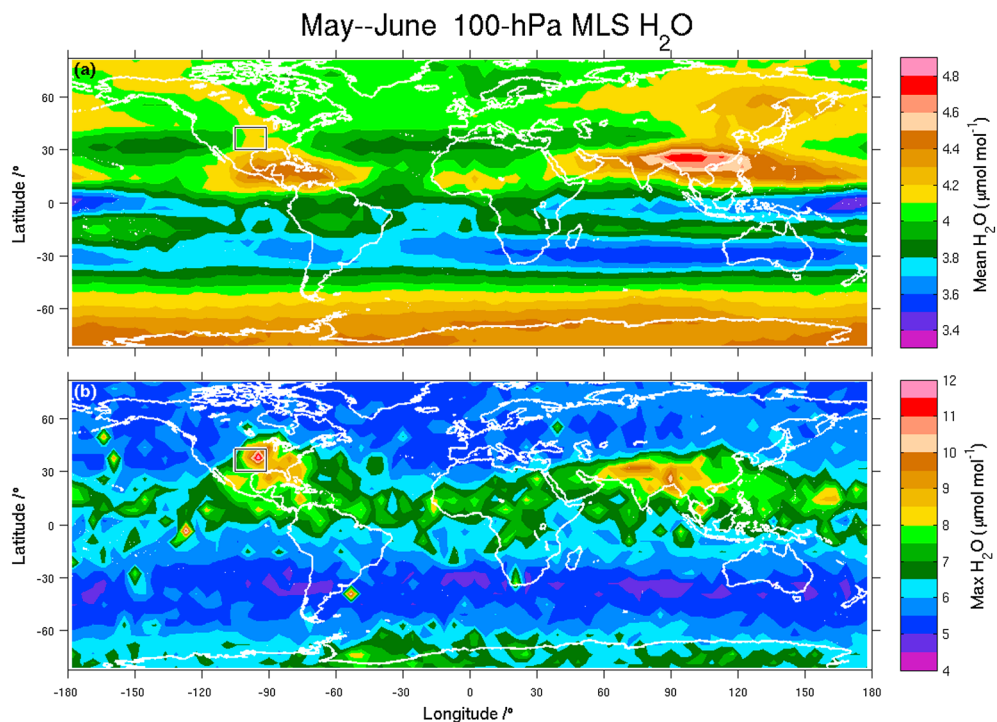


**Figure 6.** Water vapor at 100 hPa ( $\sim$ 16 km): (a) global distribution of mean and (b) maximum  $\text{H}_2\text{O}$  mixing ratios (in  $\mu\text{mol mol}^{-1}$ ) based on 10 years (2005–2014) of Aura Microwave Limb Sounder (MLS) observations for the months May–June. The operation area of the Falcon during DC3 is marked with a black box covering  $30^\circ$  to  $43^\circ\text{N}$  and  $105^\circ$  to  $91^\circ\text{W}$ .

$\text{LNO}_x$  with stratospheric air masses was observed. Further evidence for the frequent convective injection into the lowermost stratosphere is presented next based on a water vapor satellite measurements performed independently of the DC3 field experiment.

#### 4.2. $\text{H}_2\text{O}$ in the Lowermost Stratosphere

A climatology based on global satellite-borne water vapor measurements (Aura MLS) was compiled for the DC3 region and time period to evaluate this region with respect to injection of tropospheric air into the lowermost stratosphere.

In Figures 6a and 6b global distributions of mean and maximum  $\text{H}_2\text{O}$  mixing ratios at 100 hPa for the DC3 time period (May–June) are shown. The 100 hPa level ( $\sim$ 16 km) was selected since it is located well above the primary tropopause and its transition region ( $\sim$ 11–15 km). The figures are filled contour plots of gridded data including all MLS measurements for the time periods indicated. In Figure 6a the dominating  $\text{H}_2\text{O}$  features in the 10 year climatology of mean values are, as expected, elongated areas of enhanced  $\text{H}_2\text{O}$  along the Intertropical Convergence Zone (ITCZ), especially over central Asia and Central America. Interestingly, the global distribution of maximum  $\text{H}_2\text{O}$  mixing ratios at 100 hPa shows that  $\text{H}_2\text{O}$  is not only enhanced along the ITCZ, but the highest values ( $12 \mu\text{mol mol}^{-1}$ ) are observed over parts of the DC3 region over the Central U.S. probed by the Falcon (indicated by the black box in Figure 6b). The highest  $\text{H}_2\text{O}$  values in Figure 6b are located in the eastern part of the black box and farther northeastward, which is probably the result of advected anvils from intense thunderstorms formed in the Tornado Alley (e.g., northern Texas, Oklahoma, Kansas, and eastern Colorado). Previous analyses of the same data set on an annual basis already showed that convective events with enhanced  $\text{H}_2\text{O}$  in the UT/LS region are especially frequent over the U.S. and central Asia [Schwartz et al., 2013].

To determine if these elevated  $\text{H}_2\text{O}$  events were especially pronounced over the Central U.S. during the DC3 time period in May–June 2012, the 10 year  $\text{H}_2\text{O}$  data set was separated into single annual distributions (2005–2014) averaged over the months May–June. A  $\text{H}_2\text{O}$  maximum over the Central U.S. is obvious for most years in May–June (Figures 7a–7j). In addition, the  $\text{H}_2\text{O}$  distribution in May–June 2012 shows an especially

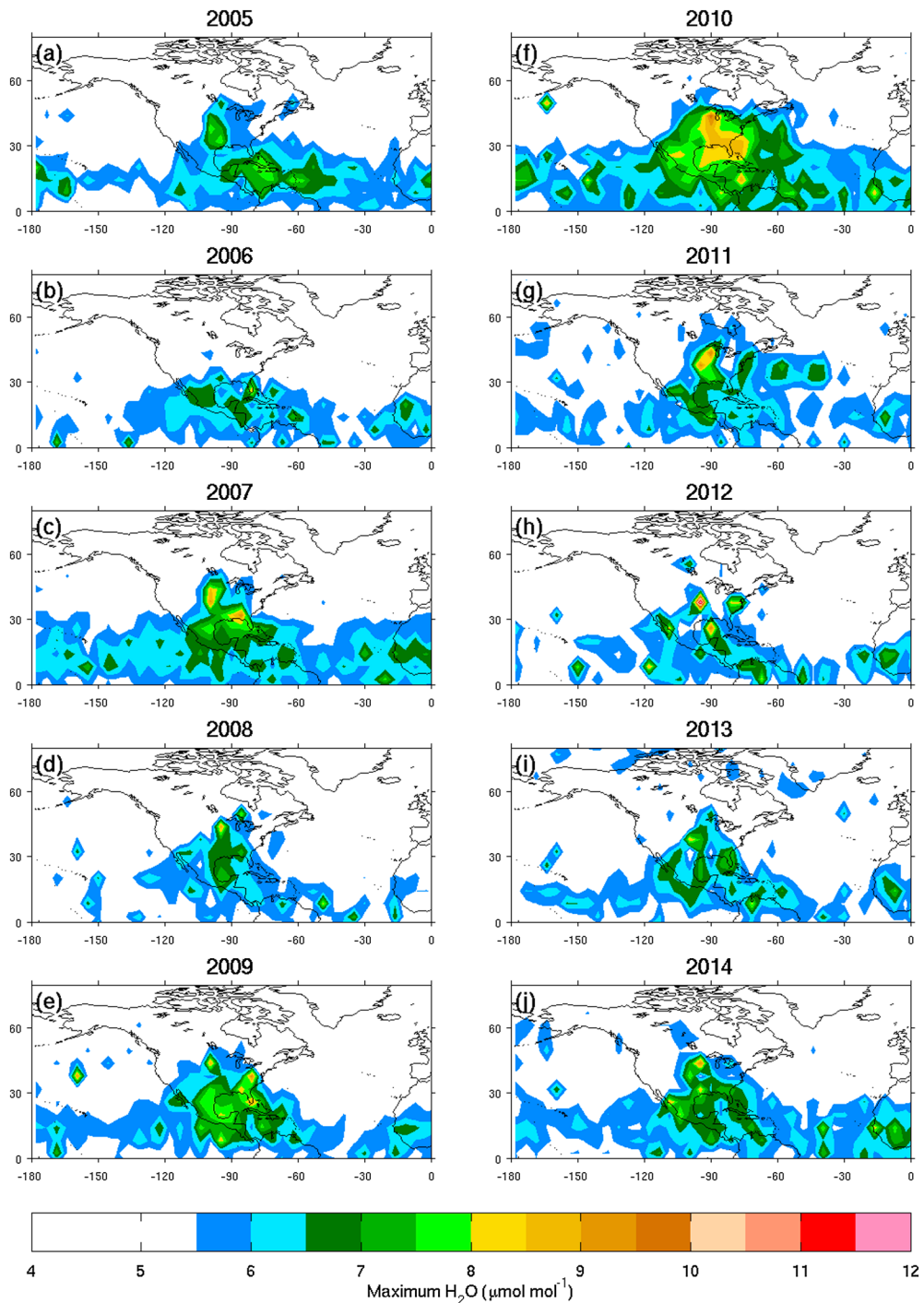


**Figure 7.** (a–j) Water vapor at 100 hPa (~16 km): maximum H<sub>2</sub>O mixing ratios (in  $\mu\text{mol mol}^{-1}$ ) for the months May–June based on Aura Microwave Limb Sounder (MLS) observations for the years 2005–2014 centered over North America.

strong but not very extended H<sub>2</sub>O maximum over the Central U.S. (Figure 7h). One explanation for the frequent occurrence of convectively transported water vapor in the LMS over this region has recently been given by Homeyer *et al.* [2014]: poleward Rossby wave breaking was suggested to cause large-scale double-tropopause events. As a result the reduced stability in the LMS may support the development of overshooting thunderstorms and the convective injection of H<sub>2</sub>O to the LMS. Observations by Wang [2003] and Anderson *et al.* [2012] indicate that a high frequency of the deep convective events in midlatitudes may penetrate into

the LMS, especially impacting the H<sub>2</sub>O budget. Our measurements during DC3 confirm the high frequency of such events over the Central U.S. as also shown in section 5.

A further explanation for the midlatitude wetness in the LMS over the Central U.S. could also be attributed to the horizontal transport of H<sub>2</sub>O from the tropics as suggested by, e.g., Jiang *et al.* [2012, 2015]. This in mixing is known to be a quasi-isentropic transport [Konopka *et al.*, 2009; Ploeger *et al.*, 2012]. Most likely, both this horizontal transport and overshooting convection contribute to the enhanced H<sub>2</sub>O mixing ratios in the LMS over the Central U.S. in May–June. MLS studies on the diurnal variation of H<sub>2</sub>O and ice water content in the LMS are in preparation to quantify the contribution from direct convective injection (M. Schwartz, personal communication, 2016). Furthermore, MLS measurements in the LMS indicate that high H<sub>2</sub>O mixing ratios extend into the Upper Midwest, farther north and east than predicted by present models [e.g., Schoeberl *et al.*, 2013], which is consistent with our airborne observations indicating a major contribution from convective injection in this region. Recent global Atmospheric Chemistry Experiment Fourier transform spectrometer (ACE-FTS) HDO/H<sub>2</sub>O (i.e., δD) measurements show that the direct convective injection from the BL plays an important role in controlling the H<sub>2</sub>O isotopic composition during, e.g., the North American summer monsoon [Randel *et al.*, 2012]. Furthermore, Liu and Zipser [2015] analyzed precipitation radar data on board the Global Precipitation Mission core satellite and found that the thunderstorm systems over the Great Plains belong to the deepest precipitation systems worldwide. The global occurrence of this type of extreme systems is rare, but they were found to play an important role in the global water cycle.

## 5. Severe Convection Case on 29 May 2012 Over Texas/Oklahoma

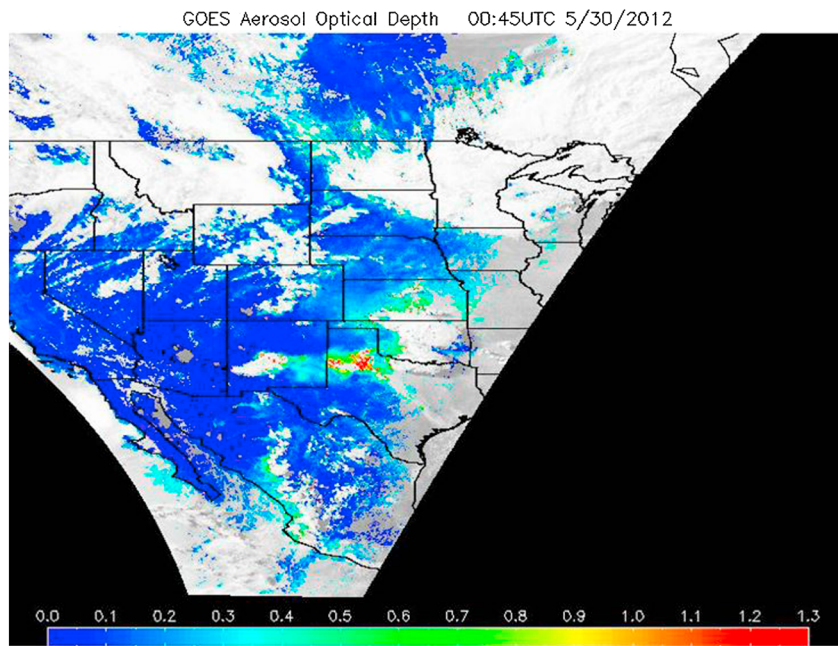
Next a case study is presented focusing on a severe convection case on 29 May 2012 over Texas/Oklahoma where deep convective clouds developed with overshooting tops. This was the first mission day for the Falcon aircraft, and it was a joint flight with the DC8 and GV aircraft. The objective here is to give a first glance of typical observations made during DC3, especially to give an impression of the strength of the observed DC3 storms and their impact on the trace species (O<sub>3</sub> and aerosol) composition in the UT/LS region. Thereby, a number of interesting observations concerning the transport mechanisms redistributing trace species inside and near thunderstorms were made that will be discussed in this section.

This successful DC3 flight is also discussed by Pollack *et al.* [2016] and Cummings *et al.* [2014] in their studies focusing on the quantification of LNO<sub>x</sub> during DC3 and on the verification of the Weather Research and Forecasting (WRF)-Chem flash rate parameterization schemes with NLDN and Lightning Mapping Array (LMA) flash rates. Furthermore, this flight is discussed by Barth *et al.* [2015], Bela *et al.* [2016], A. Fried *et al.* (Convective transport and scavenging of formaldehyde to the upper troposphere and lower stratosphere in thunderstorms over the Central United States during the 2012 DC3 study, in preparation for *Journal of Geophysical Research Atmospheres*, 2015), and Yang *et al.* [2015] for wet scavenging of soluble trace gases and aerosols.

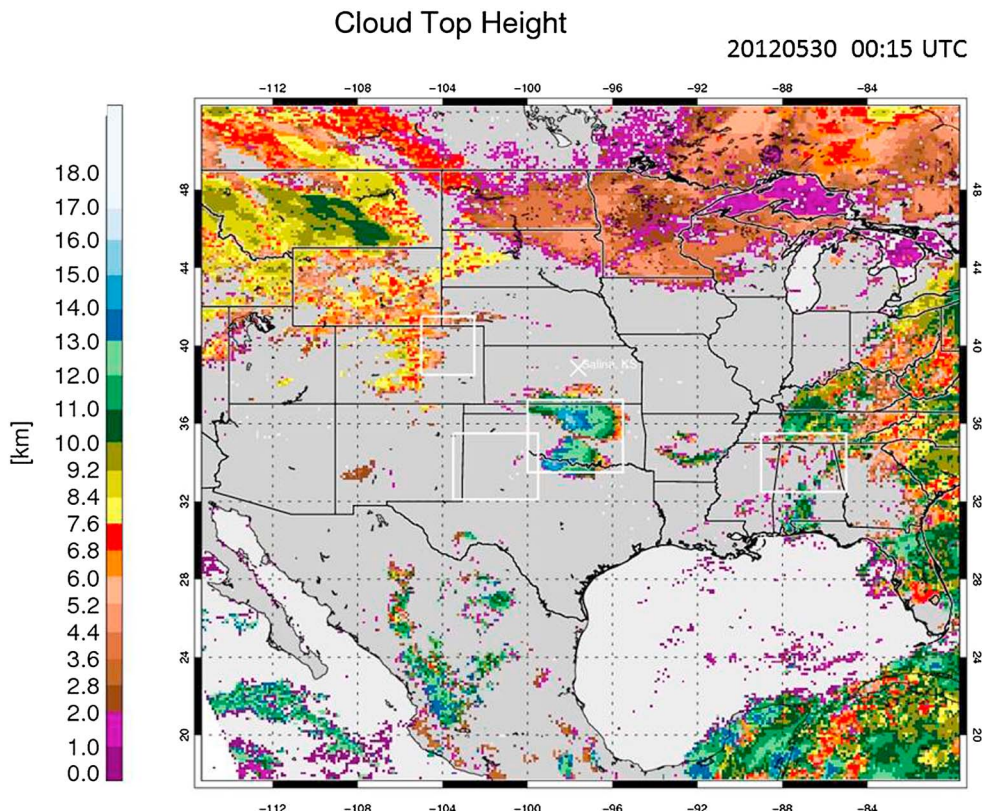
### 5.1. General Observations With Focus on Falcon In Situ Measurements

On 29 May 2012 the Falcon performed two flights. The first one was dedicated to the smoke plume from the Whitewater-Baldy wildfire in New Mexico with a brief refueling stop in Lubbock (TX). Increasing rBC mass mixing ratios with altitude were measured from the ground to the mid troposphere (Figure 2e), with a maximum value at ~4 km exceeding 1400 ng kg<sup>-1</sup> (Table 4). Near Lubbock two VOC probes were taken within this BB plume at ~4 km altitude (at 76,740 s and at 79,110 s). Ethane mixing ratios in the two probes were strongly enhanced (3013 and 5277 pmol mol<sup>-1</sup>) and also propane mixing ratios (1989 and 4819 pmol mol<sup>-1</sup>). Figure 8 shows the smoke plume spreading eastward over the Texas Panhandle and toward Oklahoma. The predominant AOD signal surrounding the thunderstorms over Texas/Oklahoma was from the Whitewater-Baldy Fire; however, the northernmost side of the storm system was likely also impacted by emissions from the Little Sand Fire in southern Colorado.

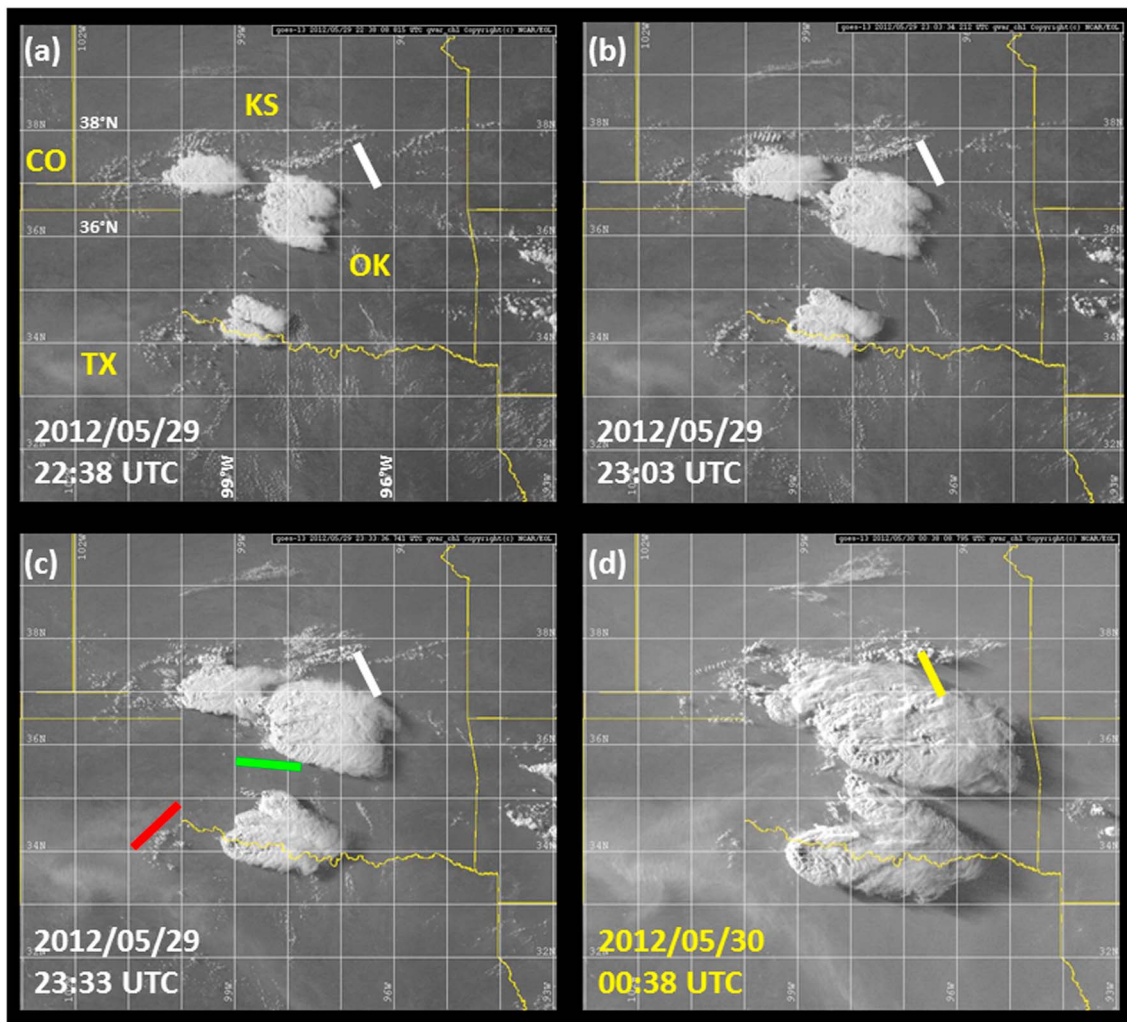
During the second flight, strongly enhanced SO<sub>2</sub> mixing ratios up to 2.6 nmol mol<sup>-1</sup> (Table 4) were measured within the dense smoke plume (AOD ~1.3) as the aircraft ascended from Lubbock. The mean vertical SO<sub>2</sub> profile shows that the plume reached up to ~5 km altitude (Figure 2b). Unfortunately, no rBC measurements were available for this flight and only one VOC probe in the UT/LS background. The main objective of the second flight was to probe the anvil outflow from a line of isolated supercell storms over Oklahoma together with the DC8 and GV aircraft.



**Figure 8.** GOES aerosol optical depth (AOD) over U.S. and Canada on 30 May 2012 at 00:45 UTC. The smoke plume from the New Mexico Whitewater-Baldy wildfire is advected to the east over the Texas Panhandle and surrounds the probed thunderstorms over Oklahoma.

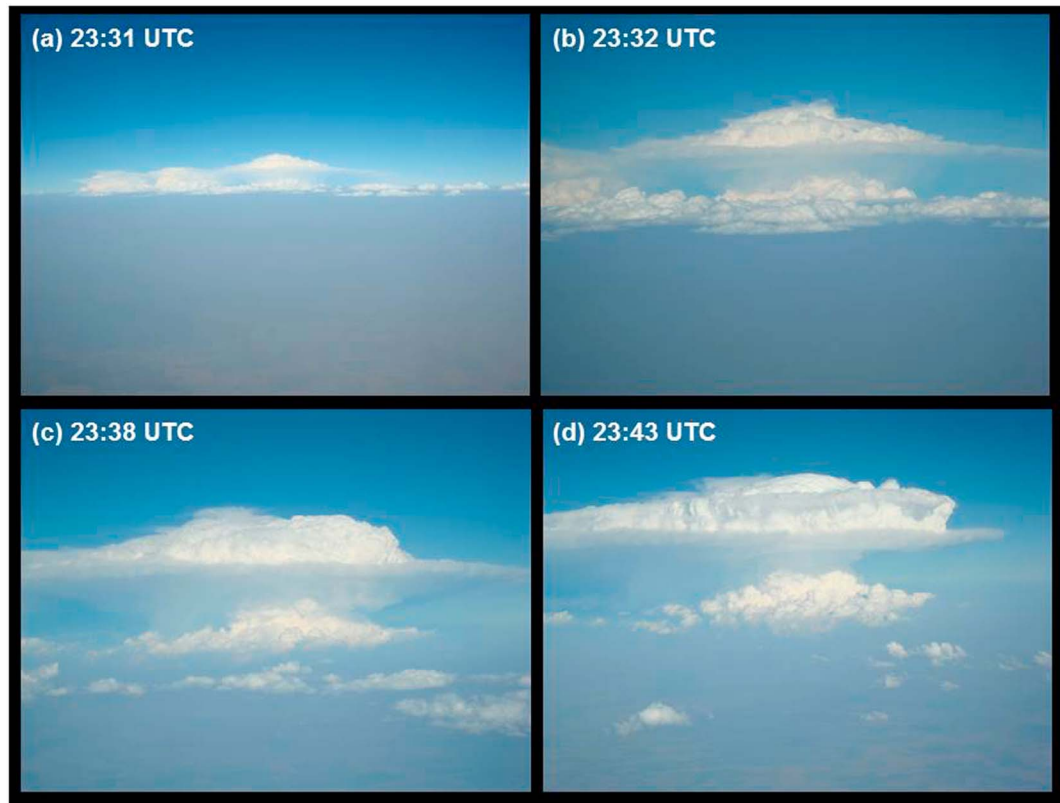


**Figure 9.** Cloud top heights (in km) derived from GOES data on 30 May 2012 at 00:15 UTC. The white squares mark the selected DC3 operation areas and the white cross the campaign base in Salina.



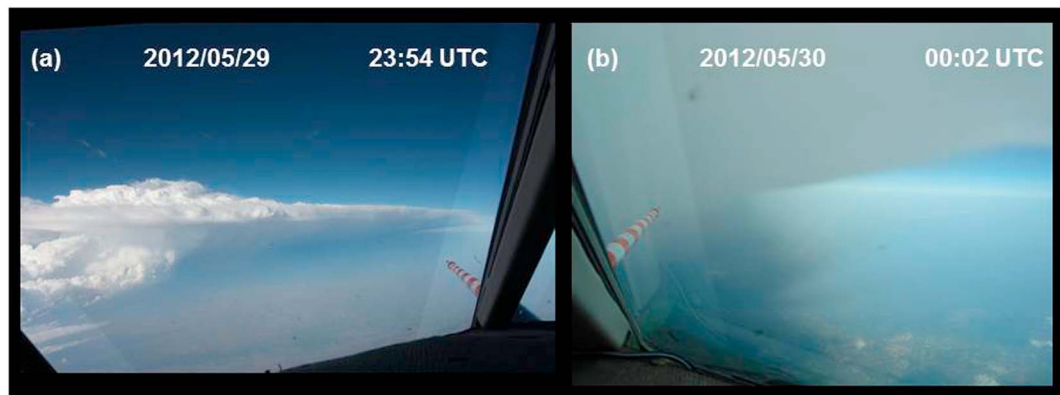
**Figure 10.** GOES visible satellite images on 29 May 2012 (a) at 22:38 UTC, (b) at 23:03 UTC, and (c) at 23:33 UTC and (d) on 30 May 2012 at 00:38 UTC (© NCAR/EOL). The colored bars indicate highlighted time periods where Falcon photos (red/green bars; see Figures 11 and 12) and Falcon/DC8 measurements (yellow bar; see Figures 15 and 16) are described in the text. The white bars coincide with the yellow bar and are used for orientation purposes.

In the evening of 29 May, several intense thunderstorm systems developed over Texas and Oklahoma along the dry line. Cloud top heights derived from GOES 13 at 23:45 UTC (29 May, not shown) and at 00:15 UTC (30 May, Figure 9) indicate that the cloud deck of the main anvil outflow was growing rapidly from ~11–12 km to ~12–13 km and the overshooting tops grew from ~15 km to 16 km. One hour later, the overshooting tops even reached ~17–18 km in agreement with NEXRAD radar data (not shown). The 00 UTC radiosoundings from Fort Worth (TX) near Dallas and Norman (OK) indicate that the primary tropopause was located at ~11.0–11.5 km ([http://catalog.eol.ucar.edu/cgi-bin/dc3\\_2012/ops/index](http://catalog.eol.ucar.edu/cgi-bin/dc3_2012/ops/index)) in agreement with Falcon temperature profile measurements (not shown), and a secondary and third “tropopause” (weak capping of temperature) is visible at ~13.5–14.0 and ~15.0–16.0 km, respectively. Farther to the north the soundings from Lamont (border Oklahoma-Kansas) at 17 UTC (29 May) and 06 UTC (30 May) indicated that the height of the primary tropopause rose during the afternoon and evening from ~10 km to ~12 km. In addition, a Mobile GPS Advanced Upper-Air Sounding System (MGAUS) was operated by the National Severe Storms Laboratory (NSSL) who released a radiosonde in the prestorm environment (35.67°N, 98.34°W). The sounding from 20 UTC indicated a primary and secondary tropopause at ~11 and ~13 km, respectively (<http://data.eol.ucar.edu/>). Tropopause heights were also available from NCEP Global Forecast System-Final (GFS-FNL) model analyses (6-hourly,  $1^\circ \times 1^\circ$  grid) interpolated to the Falcon aircraft position and time (<http://catalog.eol.ucar.edu/dc3/>). These analyses indicate a primary tropopause height distinctly higher at ~16–17 km. Overall, the measurements and the model analyses indicated a wide tropopause transition zone in the vicinity of the storms between ~11 and ~17 km altitude.

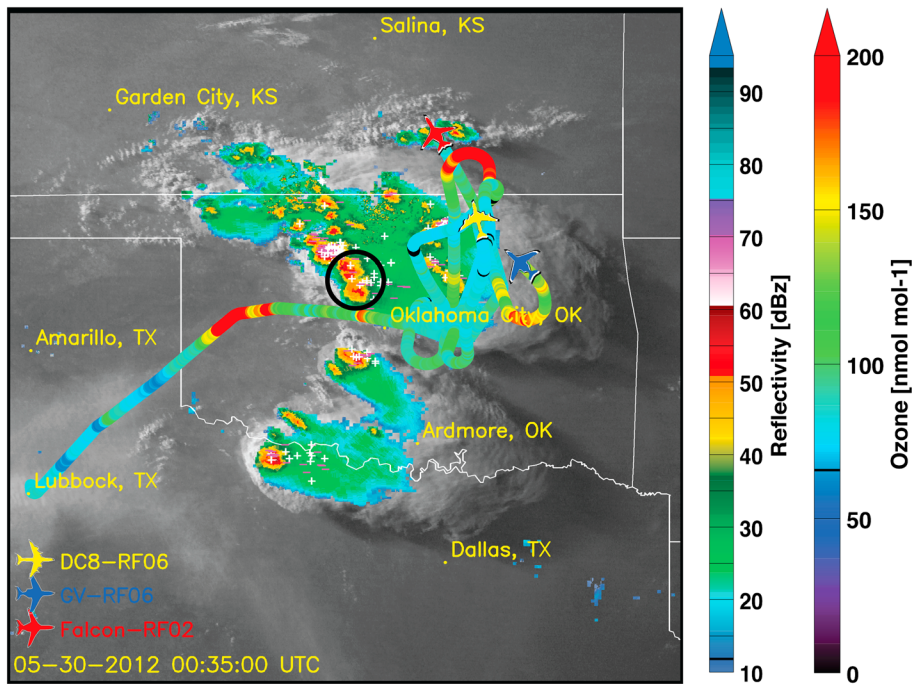


**Figure 11.** Falcon flight on 29 May 2012: view from the cockpit at (a) 23:31 UTC, (b) 23:32 UTC, (c) 23:38 UTC, and (d) 23:43 UTC. Along the border between Texas and Oklahoma, in a polluted air mass impacted by the smoke plume from the New Mexico Whitewater-Baldy Fire, a rapidly growing supercell developed with a double-decker outflow (Photo: R. Welser, DLR).

The rapid cloud development in the evening on 29 May is shown in Figures 10a–10d. The NW flow advected the anvils to the ESE. The southernmost system consisted of three supercells aligned in north-south direction at the border between Texas and Oklahoma. This convective line was not probed in situ by any of the aircraft. However, the strong intensity of the three supercells was observed from the Falcon cockpit (Figures 11a–11d). The photos were taken after the takeoff from Lubbock when the aircraft headed to the NE (red bar in Figure 10c). The presence of the Whitewater-Baldy smoke plume (brownish layer below cruise altitude) is clearly visible in Figure 11a, as well as in the satellite images (Figure 10d, lower left). The southernmost supercell is enlarged in



**Figure 12.** Falcon flight on 29–30 May 2012: view from the cockpit (a) on 29 May at 23:54 UTC and (b) on 30 May at 00:02 UTC. The lower boundary of the anvil outflow from severe convection over Oklahoma was probed. (Photo: R. Welser and A. Minikin, DLR).



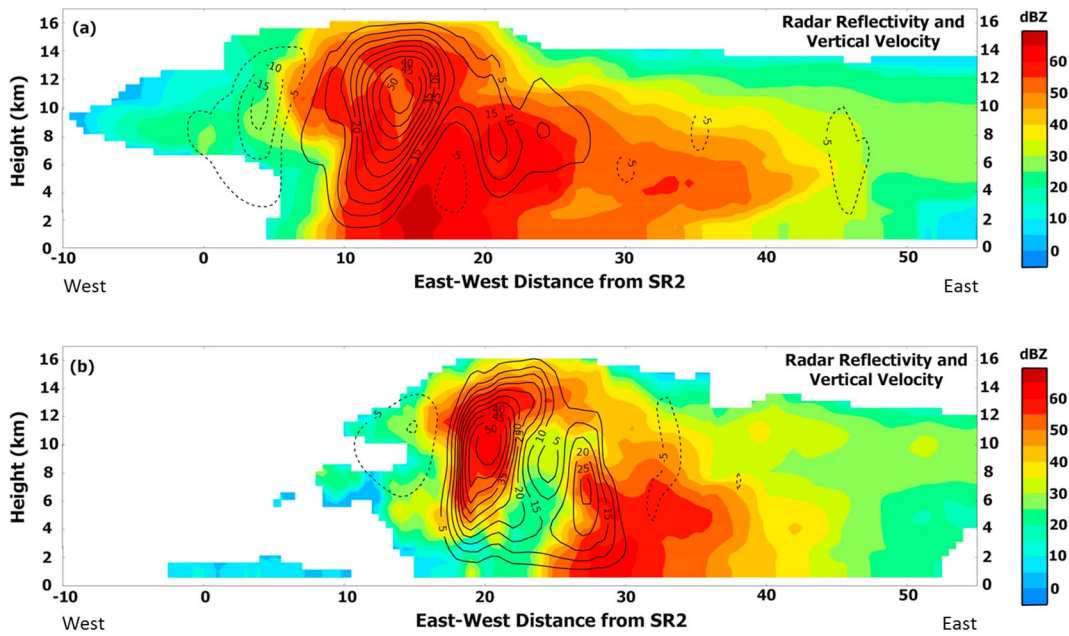
**Figure 13.** A joint flight of the Falcon (red aircraft), DC8 (yellow aircraft), and GV (blue aircraft) in the evening on 29 May to probe a line of isolated supercell storms over Oklahoma. The flight tracks (color coded according to measured O<sub>3</sub> mixing ratios) are superimposed on a GOES IR satellite image (grey), NEXRAD radar reflectivity (colored clouds), and NLDN lightning data (white/pink plus/minus sign for positive/negative flashes) from 30 May at 00:35 UTC. The Falcon flight (b flight) with start from Lubbock is shown. In addition, portions of the DC8 and GV flight tracks for the last hour are superimposed. The smoke plume from the New Mexico Whitewater-Baldy Fire is visible near Lubbock. The black circle highlights the two supercells measured by the SMART radars as shown in Figures 14a and 14b.

Figure 11d. The anvil outflow of this storm had a double-decker structure in the shape of a broad and persistent overshooting top (“anvil dome”), shaped during the crossing of the primary and secondary tropopause.

The Falcon continued heading northeastward along the dry line and passed through a narrow gap between the southern and northern line of supercells over Oklahoma. The probing of the anvil outflow started (green bar in Figure 10c). A view from the cockpit in Figure 12a confirms that the supercells developed an overshooting top as described before. When the Falcon reached the northern convective line, the DC8 and GV aircraft were already probing the front side of the line, the eastern outflow as shown in Figure 13. DC8 and GV reported that the vertical extension of the main anvil outflow was located at 10.4–11.3 km which was below the primary tropopause according to the sounding measurements described before.

An analysis of SMART radar data indicated that the cloud deck of the main anvil outflow was located slightly higher as illustrated in Figures 14a and 14b. The E-W vertical cross section of SMART radar data is shown for the two southernmost storm cells probed by the aircraft (marked by the black circle in Figure 13). Here the main anvil outflow reached up to ~12–13 km (coinciding with the secondary tropopause). The overshooting tops reached up to ~18 km (located just above the third tropopause); however, in Figures 14a and 14b the radar analysis topmost altitude is 16 km. Maximum updrafts within the storm cells were very strong and exceeded 50 m s<sup>-1</sup> near the tropopause layer around 11–12 km.

Around 00 UTC, the Falcon approached the rear side of the northern convective line. First, a stratospheric intrusion was passed with O<sub>3</sub> mixing ratios as high as 180 nmol mol<sup>-1</sup> (Figure 13). Thereafter, the lower boundary of the anvil outflow was probed at 10.7 km (Figure 12b). During the penetration to the front side of the convective line, ozone mixing ratios varied between ~80 and 100 nmol mol<sup>-1</sup> inside the anvil outflow as measured by all three aircraft (Figure 13). In Figure 15 measured O<sub>3</sub> mixing ratios along the Falcon flight path are shown in more detail: as horizontal longitude/latitude, vertical longitude/altitude, and vertical altitude/latitude distributions. Unfortunately, CO measurements are not available for this flight (see Table 2). Inside the anvil outflow O<sub>3</sub> mixing ratios are distinctly lower than observed before along the edge of the



**Figure 14.** Radar reflectivity (dBZ) (colored) and vertical velocity ( $\text{m s}^{-1}$ ) (black isolines) obtained from multi-Doppler analyses of data from the SMART radars on 30 May 2012 at 0000 UTC. Vertical cross sections (east-west) of two storm cells embedded in the line of isolated supercells probed by the Falcon in Figure 13 (located north of Oklahoma City). The grid center is the location of the SR2 radar ( $35.8^\circ\text{N}$ ,  $98.3^\circ\text{W}$ ). (a) The supercell located just north of the supercell passed by the Falcon in Figure 13 is shown. (b) The supercell passed by the Falcon in Figure 13 is shown.

anvil outflow at the same altitude by the Falcon. However, the in-cloud values are within the range of mean  $\text{O}_3$  mixing ratios ( $\sim 90 \text{ nmol mol}^{-1}$ ) observed at this altitude during the campaign (Figure 2d). In the LT, mixing ratios varied between  $\sim 70$  and  $80 \text{ nmol mol}^{-1}$  during this flight. The lower  $\text{O}_3$  values observed within the anvil outflow (down to  $\sim 80 \text{ nmol mol}^{-1}$ ) were influenced by air masses transported upward from the LT,

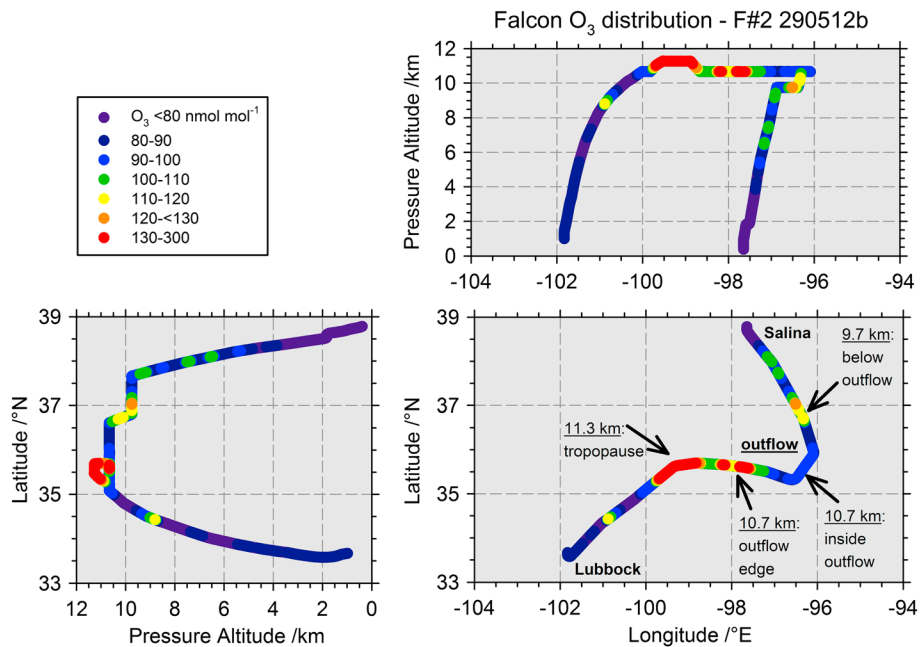


**Figure 15.** Distribution of  $\text{O}_3$  mixing ratios along the Falcon flight path on 29 May 2012 from Lubbock (TX) to Salina (KS): (bottom right) longitude/latitude distribution, (top right) longitude/altitude distribution, and (bottom left) altitude/latitude distribution. The flight was performed from the rear to the front side of a convective line of isolated supercell storms.

which is confirmed by the strong updrafts illustrated in Figures 14a and 14b. The higher O<sub>3</sub> values observed along the edges of the anvil outflow coincide with pronounced downdrafts ( $\sim 15 \text{ m s}^{-1}$ ), suggesting that O<sub>3</sub>-rich air masses from above (stratosphere) mixed into the anvil outflow.

At 00:25 UTC (latitude 36.8°N, longitude 96.4°W) the Falcon descended down to 9.7 km just below the anvil outflow, and O<sub>3</sub> mixing ratios increased up to  $\sim 100\text{--}120 \text{ nmol mol}^{-1}$  (Figure 15). These mixing ratios are well above the mean values observed at this altitude ( $\sim 90 \text{ nmol mol}^{-1}$ ) and give a possible indication of a lower located tropopause and/or wrapping of O<sub>3</sub>-rich air from the stratosphere around the anvil outflow, as observed by *Pan et al.* [2014] in the vicinity of the 30 May MCS over Kansas during DC3.

The aircraft remained at this cruising altitude until 00:34 UTC (latitude 37.7°N, longitude 96.9°W). The large O<sub>3</sub> gradients in the anvil outflow region between in cloud and out of cloud were also observed by the DC8 and GV aircraft (Figure 13). Ozone mixing ratios measured by the GV (up to  $\sim 220 \text{ nmol mol}^{-1}$ ) north and south-east of the convective line were slightly higher compared to the Falcon measurements on the western (rear) side of the convective line. The GV was flying at altitudes just above the primary tropopause at  $\sim 11\text{--}12 \text{ km}$  influenced by stratospheric air masses. The tropopause height surrounding the storm was most likely located lower compared to above the storm and caused this strong vertical and horizontal gradient in O<sub>3</sub> (multiple tropopause structure as described before).

## 5.2. DC8 Remote and In Situ Measurements

Almost simultaneously with the Falcon measurements indicated by the yellow bar in Figure 10d (at 00:25–00:34 UTC), lidar and in situ measurements were carried out on board the DC8 (at 00:36–00:44 UTC) in the same area.

In the aerosol backscatter 532 nm image (Figure 16a, left side) the anvil outflow boundaries are indicated with the white colors surrounded by pronounced red and yellow gradients. At this time, the top of the main anvil cloud deck reached up to  $\sim 12 \text{ km}$ , which is in agreement with cloud top heights derived from GOES 13, radar data, and tropopause heights estimated from the radiosounding mentioned before. The DC8 cruising level was at 10.7 km (black line in the lidar image). The bottom of the main anvil outflow reached down to  $\sim 9 \text{ km}$ . Aerosol backscatter was strongly enhanced (up to  $\sim 5 \text{ Mm}^{-1} \text{ sr}^{-1}$ ) from the ground up to  $\sim 5 \text{ km}$  due to the presence of the Whitewater-Baldy (and Little Sand) smoke plumes. Above the lower smoke layer, a secondary layer of enhanced aerosol backscatter (up to  $\sim 0.5 \text{ Mm}^{-1} \text{ sr}^{-1}$ ) is visible at  $\sim 7.5\text{--}8.5 \text{ km}$ . The lidar image (right side) suggests that this layer was most likely uplifted by smaller convective cells (towering cumulus along the flanking line) just north of the convective line (Figure 10d). The precipitation rate was still low within these clouds (Figure 13), causing no major washout effects. This may explain why a high ratio of aerosol backscatter is spreading out from these clouds toward, however, below the main anvil outflow of the supercells. In comparison, at the same altitude as the main anvil outflow ( $\sim 9\text{--}12 \text{ km}$ ), but outside of clouds, no large enhancement in aerosol backscatter is visible (Figure 16a). This observation suggests that the supercell outflow was dominated by efficient washout processes as also observed for other DC3 cases [*Barth et al.*, 2015; *Yang et al.*, 2015]. In addition, deep convection active earlier in the evening could also have contributed to the enhanced aerosol backscatter layer at  $\sim 7.5\text{--}8.5 \text{ km}$ .

In agreement with the observations by the Falcon at 10.7 km, lower O<sub>3</sub> mixing ratios were measured inside the anvil outflow ( $\sim 90\text{--}110 \text{ nmol mol}^{-1}$ ) compared to outside the outflow ( $\sim 120\text{--}150 \text{ nmol mol}^{-1}$ ) at 10.7 km by the in situ O<sub>3</sub> instrument on board the DC8 (Figure 16b). The lidar measurements in the same figure show that lower O<sub>3</sub> mixing ratios (down to  $\sim 90 \text{ nmol mol}^{-1}$ ) were also present along the edges of the anvil outflow at  $\sim 12 \text{ km}$  (anvil cloud deck) and  $\sim 14 \text{ km}$  (overshooting top). At these altitudes, O<sub>3</sub> mixing ratios distinctly above  $\sim 100 \text{ nmol mol}^{-1}$  are expected from the mean vertical O<sub>3</sub> profile (Figure 2d), which indicates that O<sub>3</sub>-poorer air masses from below were transported upward to the UT/LS region by the supercells. On the other hand, just outside of the anvil outflow at  $\sim 12 \text{ km}$  altitude, enhanced O<sub>3</sub> mixing ratios up to  $\sim 200 \text{ nmol mol}^{-1}$  were observed indicating downward transport of O<sub>3</sub>-rich air masses to the tropopause region and possibly below, similar to *Pan et al.* [2014] findings.

In addition, slightly enhanced O<sub>3</sub> mixing ratios (up to  $\sim 110 \text{ nmol mol}^{-1}$ ) were observed in the lofted aerosol backscatter layer at  $\sim 7.5\text{--}8.5 \text{ km}$  compared to the  $\sim 70\text{--}80 \text{ nmol mol}^{-1}$  in the lower layer. From the available measurements it is unfortunately not possible to determine the cause of the enhanced O<sub>3</sub> mixing ratios in the

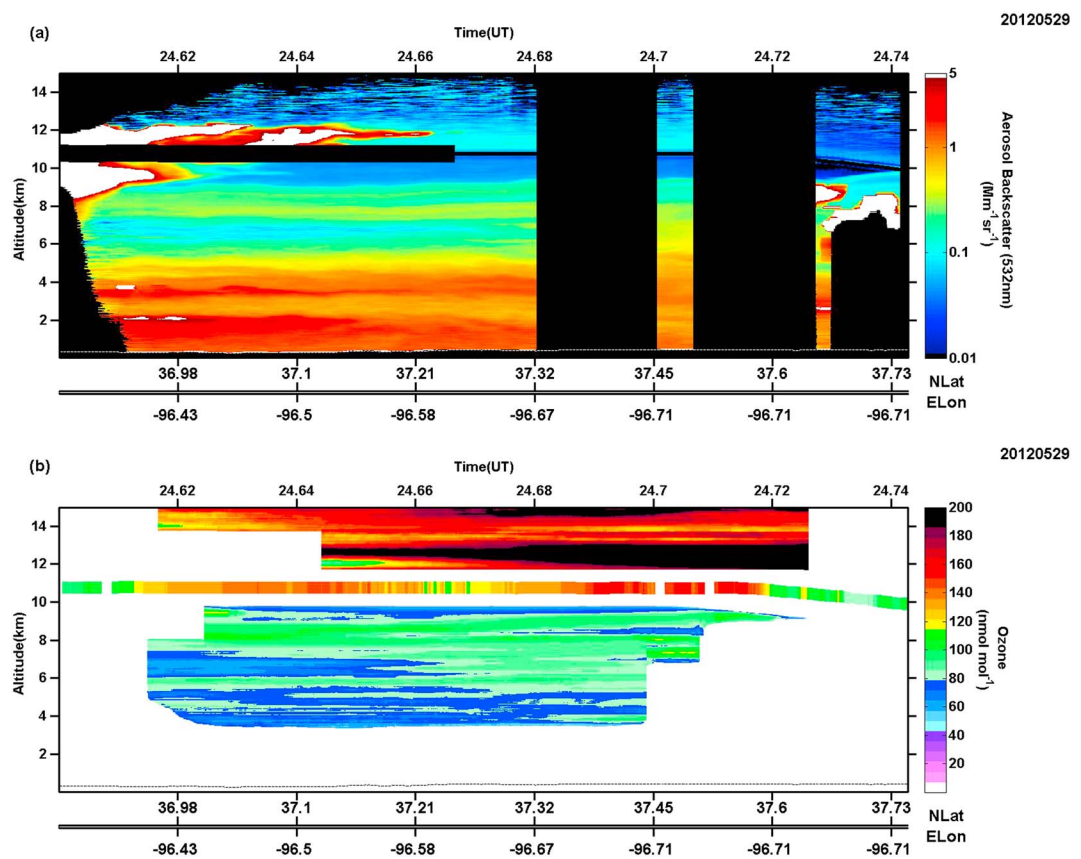


**Figure 16.** Measurements from the DC8 aircraft on 30 May 2012 at 00:36–00:44 UTC: (a) aerosol backscatter measured by lidar and (b) ozone mixing ratios measured by in situ instrumentation (thicker line between 10 and 12 km) and by lidar (2-D curtain above and below the cruising altitude).

lofted aerosol layer (photochemistry or/and stratospheric influence). In HH2016 more detailed case study analyses are presented to discuss the influence from these two  $O_3$  sources.

### 5.3. Schematic of Major Air Mass Transport Pathways Within/Around the Storm

To summarize the findings in the last two sections, a schematic presenting our hypothesis on the major air mass transport pathways within/around the probed DC3 thunderstorms is shown in Figure 17. Superimposed on an isolated supercell thunderstorm are results based on Figures 14–16 from our airborne in situ trace species and lidar measurements and ground-based radar measurements on 29 May 2012 (yellow and red arrows). In addition, more well-known pathways (green and grey arrows) as described by, e.g., Poulida *et al.* [1996] are shown. The schematic shows that emissions from wildfires (BB) are ingested into towering cumulus along the flanking line and into the major storm (yellow arrows). Strong updrafts and downdrafts (green and grey arrows) within the storm redistribute the ingested pollution. As a response to the overshooting top, stratospheric air masses are transported downward into the boundaries of the anvil outflow and/or are wrapped around the anvil outflow (red arrows) as observed in our measurement presented previously in this section. The latter transport pathway was also observed by Pan *et al.* [2014] in  $O_3$  lidar images during DC3. Each of the major air mass transport pathways illustrated in Figure 17 is supported by further DC3 case studies discussed in more detail in HH2016.

## 6. Summary, Discussion, and Conclusions

During the DC3 field campaign in summer 2012 over the Central U.S., a unique data set on chemical composition, dynamical, microphysical, and electrical properties within and in the vicinity of thunderstorms was obtained by three research aircraft (NASA-DC8, NSF/NCAR-GV, and DLR-Falcon) and a dense network of ground-based radars and lightning detection sensors.

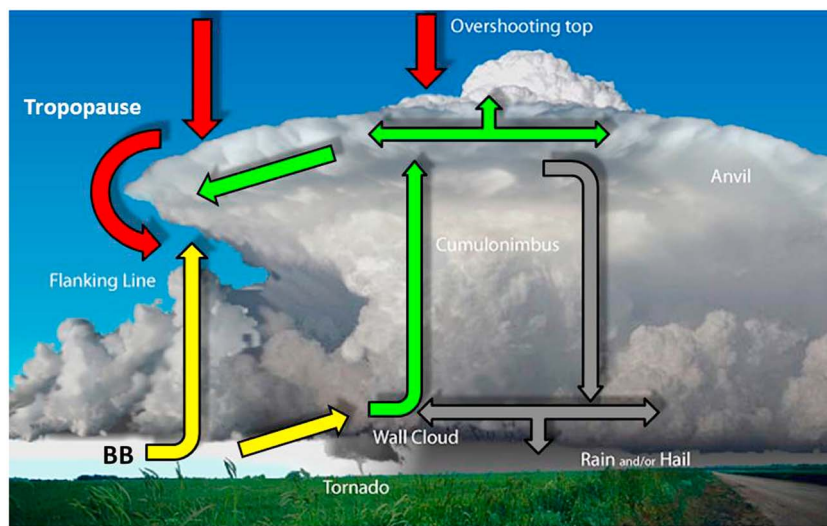


**Figure 17.** Schematic of an isolated, overshooting thunderstorm (credit: NOAA National Weather Service, <http://www.srh.noaa.gov/jetstream/tstorms/tstrmtypes.htm>). Superimposed are arrows presenting our hypothesis on the major air mass transport pathways within/around the probed DC3 thunderstorms based on joint in situ trace gas and lidar measurements (Falcon, DC8, and GV) and ground-based radar measurements. Our hypothesis suggests that emissions from wildfires (BB) are ingested into towering cumulus along the flanking line and into the major storm (yellow). Strong updrafts and downdrafts (green and grey) within the storm redistribute the ingested pollution. As a response to the overshooting top, stratospheric air masses are transported downward along the boundaries of the anvil outflow (red).

DC3 observations presented here can be summarized in the following general statements, and further details are given below.

1. Pollution from wildfires was especially strong during DC3.
2. Pollution from wildfires was ingested into the DC3 thunderstorms.
3. Lofted pollution layers from wildfires frequently surrounded the thunderstorms.
4. DC3 thunderstorms were particularly intense compared to other thunderstorms probed in the past by the Falcon over other continents.
5. DC3 thunderstorms frequently developed overshooting tops.
6. DC3 thunderstorms injected high amounts of  $H_2O$  into the lowermost stratosphere.
7. DC3 thunderstorms produced high amounts of  $LNO_x$ .
8.  $LNO_x$  frequently mixed with stratospheric air masses.
9.  $O_3$  mixing ratios were highly variable in the anvil outflow region.

The present study gave a general overview of a variety of trace species measured in situ by the DLR-Falcon aircraft ( $CO$ ,  $SO_2$ ,  $CH_4$ ,  $O_3$ ,  $NO$ ,  $NO_x$ , and black carbon). In addition,  $H_2O$  measurements from the Aura MLS sensor were analyzed for the DC3 period. The main focus of the general overview was on the influence of emissions from wildfires and  $LNO_x$  on the trace species composition in the UT/LS region. In addition, a case study from 29 May 2012 was presented, where a joint flight with the U.S. aircraft was performed inside and nearby a line of isolated supercell storms. Measurements from the DC8 lidar, as well as Falcon, DC8, and GV trace species in situ instruments in the thunderstorm inflow and outflow region in conjunction with ground-based radar measurements, were analyzed to give a first glance of typical observations during DC3. The selected case from 29 May 2012 very well represents a typical thunderstorm situation during the campaign, where frequently intense deep convection with overshooting tops developed over Texas/Oklahoma and occasionally over Colorado.

Besides the planned probing of intense thunderstorms (for the Falcon primarily over Texas, Oklahoma, and Colorado), coincidentally aged smoke plumes from nearby wildfires were probed ~600–1000 km downwind from the fire sources. These fires, named “Whitewater-Baldy Fire,” “Little Bear Fire,” and “High Park Fire” belong to the largest and most destructive fires in New Mexico and Colorado state’s history (Table 3). Vertical profiles of a variety of trace species (mentioned above) were analyzed to quantify the impact of these emissions from wildfires and  $LNO_x$  on the trace species composition in the UT/LS region during DC3.

In the aged wildfire plumes (~9–27 h) strongly enhanced mixing ratios of CO, SO<sub>2</sub>, and rBC were observed. Due to the long lifetime of CO and the elevated mixing ratios measured in these aged plumes (up to ~700 nmol mol<sup>-1</sup> about 1000 km downwind of the Little Bear Fire on 11 June 2012), CO (and partly SO<sub>2</sub> and rBC) emissions from wildfires turned out to be an excellent tracer for vertical transport from the BL to the UT inside and nearby the investigated thunderstorms. In comparison, CO, SO<sub>2</sub>, and rBC emissions from anthropogenic BL sources were found to be distinctly lower. Lofted plumes from BB were observed at all altitudes between the BL and ~10 km, however, most frequently in the lower and mid troposphere below ~7 km. The Falcon observed the most pronounced BB plumes on 29–30 May and 11–12 June 2012 in the vicinity of intense thunderstorms.

The anvil outflow from DC3 thunderstorms was mainly observed higher up at ~9–12 km. In cases with overshooting cloud tops, the anvil outflow spread above ~12 km according to satellite data; however, the maximum cruising altitude of the Falcon only reached up to 12.4 km. The NO<sub>x</sub> mixing ratios measured in the anvil outflow, typically ~1–3 nmol mol<sup>-1</sup>, were distinctly higher than observed on average in the BL (0.2–0.8 nmol mol<sup>-1</sup>) and mainly attributed to LNO<sub>x</sub>. The highest mean NO<sub>x</sub> mixing ratios in the anvil outflow (~3 nmol mol<sup>-1</sup>) were observed at 9.5–11.0 km in a MCS over Missouri and Arkansas on 11 June 2012. The highest NO peaks, up to 9 nmol mol<sup>-1</sup> at 9 km, were measured in a supercell over northern Texas on 30 May 2012.

Compared to past thunderstorm field campaigns performed with the Falcon over Europe (e.g., EULINOX), South America (TROCCINOX), Australia (SCOUT-O3), and West Africa (AMMA), average NO<sub>x</sub> mixing ratios in the UT/LS region (~9–12 km) were distinctly enhanced during DC3 (~1–3 nmol mol<sup>-1</sup>) and higher than observed in the above mentioned non-U.S. studies (generally <0.5 nmol mol<sup>-1</sup>). A comparison with two further thunderstorm field experiments performed by U.S. aircraft over Colorado (STERAO-A) and Florida (CRYSTAL-FACE) in the past also confirmed these especially elevated NO<sub>x</sub> mixing ratios in the UT/LS region over certain parts of the United States. The general question that arises from this finding is as follows: To what extent does the large contribution from LNO<sub>x</sub> impact the O<sub>3</sub> budget in the UT/LS region over the Central U.S.? More specifically, (1) what is the general impact of thunderstorms on the O<sub>3</sub> composition in the UT/LS region over the Central U.S.? (2) To what extent does photochemical O<sub>3</sub> production catalyzed by LNO<sub>x</sub> and stratospheric intrusions play an important role? These questions have been addressed in the past by, e.g., Cooper *et al.* [2007], Choi *et al.* [2009], and Barth *et al.* [2012] and were major tasks for our studies in the present study, as described in the next paragraph and in HH2016.

In the present study further evidence of convective injection into the UT/LS region was presented by analyzing tracer-tracer correlations (CO-NO<sub>x</sub> and O<sub>3</sub>-NO) for single Falcon flights. The CO-NO<sub>x</sub> correlation indicated that NO<sub>x</sub> mixing ratios in the BL were generally low with <1 nmol mol<sup>-1</sup> compared to the anvil outflow region (up to ~7 nmol mol<sup>-1</sup>) which was mainly impacted by LNO<sub>x</sub>. In addition, LNO<sub>x</sub> in the UT coincided with enhanced CO mixing ratios in the range of ~105–135 nmol mol<sup>-1</sup>, indicating upward transport from the LT impacted by wildfire emissions. The O<sub>3</sub>-NO correlation showed that LNO<sub>x</sub> mixed into lower stratospheric air (rich in O<sub>3</sub>) on several days (30 May and 8 and 12 June 2012), where the strong convective activity originated from supercells, MCCs, MCSs, and squall lines. Here elevated NO mixing ratios, typically ~0.3–3 nmol mol<sup>-1</sup>, coincided with elevated O<sub>3</sub> mixing ratios in the range of ~100–260 nmol mol<sup>-1</sup>. These three cases and further tracer-tracer correlations (CO-O<sub>3</sub>) are presented in HH2016. The general impact of thunderstorms on UT/LS O<sub>3</sub> composition over the Central U.S. is addressed, and the contribution of in situ O<sub>3</sub> production to stratospheric intrusions is analyzed. Furthermore, HH2016 shows more in detail how air rich (low) in O<sub>3</sub> from the stratosphere (troposphere) is being brought down (up) to the troposphere (stratosphere).

The frequent mix of LNO<sub>x</sub> with stratospheric air masses was striking during DC3. In comparison, during CRYSTAL-FACE over Florida no significant LNO<sub>x</sub> injection above the high local tropopause was observed. During STERAO-A over Colorado high O<sub>3</sub> mixing ratios were observed on the upwind side of one anvil; however, there was no evidence for entrainment into the anvil [Barth *et al.*, 2007]. In HH2016 we will give further evidence for downward mixing of O<sub>3</sub>-rich stratospheric air masses directly into the anvil outflow.

Complementary to the airborne data gained during DC3, a 10 year global climatology based on H<sub>2</sub>O remote sensing data at 100 hPa (~16 km) from the Aura MLS was constructed to evaluate the DC3 region with respect to injection of tropospheric air into the lowermost stratosphere. The data set (2005–2014) indicated that H<sub>2</sub>O

mixing ratios were especially high over the DC3 region (and farther downwind) compared to other regions at the same degree of latitude and altitude. One explanation for the frequent occurrence of convectively transported water vapor in the LMS over this region has recently been given by Homeyer *et al.* [2014]: *poleward Rossby wave breaking was suggested to cause large-scale double-tropopause events*. As a result the reduced stability in the LMS may support the development of overshooting thunderstorms and the convective injection of H<sub>2</sub>O to the LMS as we observed during DC3. Furthermore, the quasi-isentropic transport of H<sub>2</sub>O from the tropics may also enhance H<sub>2</sub>O mixing ratios in the LMS over the Central U.S. in May–June as suggested by Jiang *et al.* [2012, 2015]. Anderson *et al.* [2012] proposed that the injection of high amounts of H<sub>2</sub>O into the LMS has the potential to cause a halogen-driven ozone depletion. However, Schwartz *et al.* [2013] found that at least for volumes appreciable compared to MLS averaging kernels, it is extremely rare to have parcels wet enough and cold enough to cross Anderson's threshold for rapid binary water-sulfate aerosol growth and ozone-destroying chemistry and also to be stratospheric enough that there is appreciable chlorine to activate and ozone to destroy. In the vicinity of the thunderstorms probed during DC3 we observed that mainly dynamical and not chemical processes controlled the O<sub>3</sub> composition in the UT/LS region, as summarized next and in HH2016.

Finally in the present paper a case study from 29 May 2012 was presented focusing on severe convection developing overshooting tops which was probed by all three aircraft. The objective was to give a first glance of the kind of observations made during DC3, especially to give an impression of the strength of the observed DC3 storms and their impact on the trace species (O<sub>3</sub> and aerosol) composition in the UT/LS region. A convective line with several supercells developed over Texas and Oklahoma and was surrounded by emissions from the Whitewater-Baldy Fire (and Little Sand Fire). A number of interesting observations concerning the thunderstorm dynamics and transport mechanisms redistributing trace species inside and near thunderstorms were made, and the interaction with wildfire emissions was studied.

1. Wildfire emissions were primarily present in two layers: BL up to ~5 km and between ~7.5–8.5 km, and aerosol backscatter was distinctly enhanced in both layers.
2. In the lower BB layer O<sub>3</sub> mixing ratios were low (~70–80 nmol mol<sup>-1</sup>).
3. The upper BB layer was partly uplifted in the vicinity of the supercell by weaker flanking convection (and/or previous convection) and enhanced in O<sub>3</sub> (up to ~110 nmol mol<sup>-1</sup>).
4. No distinct enhancement in aerosol backscatter was present in the main anvil outflow region (~9–12 km), probably due to efficient washout processes.
5. The main cloud deck of the anvil outflow reached up to ~11–13 km.
6. Overshooting tops reached up to ~17–18 km.
7. The tropopause transition zone in the vicinity of the storms was highly variable (~11–17 km).
8. Besides the primary tropopause, two weaker temperature cappings were present above.
9. Anvil outflow was in the shape of an anvil dome caused by multiple tropopauses.
10. Large O<sub>3</sub> gradients were observed in the anvil outflow region between in cloud and out of cloud.
11. O<sub>3</sub> mixing ratios were lower inside the anvil outflow (down to ~80 nmol mol<sup>-1</sup>) compared to the background (~90 nmol mol<sup>-1</sup>) due to upward transport from the LT.
12. O<sub>3</sub> mixing ratios were frequently higher outside and below the anvil outflow (up to ~100–200 nmol mol<sup>-1</sup>) compared to the background (~90 nmol mol<sup>-1</sup>) due to a lower located tropopause and/or downward mixing of O<sub>3</sub>-rich air from the stratosphere, as observed by Pan *et al.* [2014] for another DC3 case.
13. The back-sheared anvil upper level downdraft was found to be a ubiquitous feature throughout the hour-long multi-Doppler analysis of two investigated supercells.

The impression from these first Falcon measurements during DC3 is that the downward (upward) transport of O<sub>3</sub>-rich (O<sub>3</sub>-poor) air masses may play an important role in increasing (decreasing) upper tropospheric (lower stratospheric) O<sub>3</sub> in the vicinity of thunderstorms. Until now, the main focus of this type of studies was more on photochemical O<sub>3</sub> production and it was thought to be the dominating process causing O<sub>3</sub> enhancements in the UT in the aged thunderstorm outflow [e.g., Cooper *et al.*, 2009]. However, recently published measurements with the DC8 O<sub>3</sub>-lidar during DC3 have shown that the downward transport of O<sub>3</sub>-rich air from the stratosphere nearby thunderstorms with overshooting tops is an important transport mechanism not considered in this extent until now [Pan *et al.*, 2014]. This pronounced transport mechanism in the vicinity of thunderstorms was also observed during a number of other Falcon DC3 flights (e.g., 30 May and 8 and 12 June) addressed in HH2016.

Results from both remote and in situ airborne measurements during DC3 show that thunderstorms over the Central U.S. generally cause a stronger redistribution of LNO<sub>x</sub>, H<sub>2</sub>O, O<sub>3</sub>, and aerosols in the UT/LS region than previously thought. This result is in agreement with, e.g., Heggen et al. [2004] who hypothesized that extratropical deep convection may have a larger influence on the chemical composition of the lowermost stratosphere than claimed by cloud-resolving models at that time.

Due to the extraordinary wide horizontal and vertical extension of thunderstorm anvils in the Central U.S. area (several hundreds of kilometers and up to ~17–18 km, respectively), in addition to their frequent daily occurrence in the summer season (April–August), it is important to consider this type of mesoscale convection in future climate model studies focusing on the chemical composition (especially O<sub>3</sub>) in the UT/LS region. We highly recommend further combined, high-resolution model and airborne in situ studies (including lidar measurements) in the UT/LS region over the Central U.S. combined with ground-based radar measurements on this important topic, especially within the perspective of increasing global temperatures, frequency of severe thunderstorms, and wildfire activity [Simmonds et al., 2005; Turetsky et al., 2011; Brooks, 2013; Romps et al., 2014].

#### Acknowledgments

The DC3 field campaign was established by a collaborative effort of NCAR, NASA, the U.S. university community, NOAA, and DLR. The National Science Foundation (NSF), NASA, NOAA, and DLR were the primary funders for DC3. NCAR is supported by the NSF. Detailed information on the scientific goals and a link to the field data is available from the DC3 website, [https://www.eol.ucar.edu/field\\_projects/dc3](https://www.eol.ucar.edu/field_projects/dc3). We greatly acknowledge the excellent collaboration with the DC3 principal investigators and all the support the DLR team received during the field phase from M.C. Barth (NCAR), C.A. Cantrell (University of Colorado), W.H. Brune (Pennsylvania State University), S.A. Rutledge (Colorado State University), and J.H. Crawford (NASA/LaRC). Furthermore, the logistical support from NCAR-EOL by V. Salazar, J. Moore, G. Stossmeister, and B. Baeuerle is greatly appreciated. We thank the Falcon pilots (R. Welser and P. Weber), A. Hausold for the logistics, the engineers and scientists of the DLR flight department for the excellent support during the field phase, and the DC8 pilots for their great collaboration during the intercomparison flight. We are grateful to G. Diskin (NASA Langley Research Center) for providing CO data from the intercomparison flight. We express our gratitude to the DLR and NCAR colleagues who supported the airborne measurements, U. Schumann, D. Fütterer, J. Kim, A. Reiter, A. Roiger, H. Ziereis, T.L. Campos, F.M. Flocke, D.J. Knapp, D.D. Montzka, and A. Schanot, and the financial support from the Deutsche Forschungsgemeinschaft (DFG, project MI 583/4-1). The ETH Zurich (T. Peters) is greatly acknowledged for providing the NO instrument. The GOES data were provided by NCAR/EOL under sponsorship of the National Science Foundation (<http://data.eol.ucar.edu/>). We thank L.L. Pan and C.R. Homeyer (NCAR Boulder) for their fruitful discussions and for providing tropopause heights from NCEP GFS-FNL model analyses. Finally, we are grateful to A. Roiger (DLR), K.A. Cummings (University of Maryland College Park), K.E. Pickering (NASA Goddard Space Flight Center Greenbelt), and to the three anonymous reviewers for their helpful comments and suggestions, which greatly helped to improve the manuscript.

#### References

- Allen, D., K. E. Pickering, B. Duncan, and M. Damon (2010), Impact of lightning NO emissions on North American photochemistry as determined using the Global Modeling Initiative (GMI) model, *J. Geophys. Res.*, 115, D22301, doi:10.1029/2010JD014062.
- Anderson, J. G., D. M. Wilmouth, J. B. Smith, and D. S. Sayres (2012), UV dosage levels in summer: Increased risk of ozone loss from convectively injected water vapor, *Science*, 337, 835–839, doi:10.1126/science.1222978.
- Andreae, M. O., D. Rosenfeld, P. Artaxo, A. A. Costa, G. P. Frank, K. M. Longo, and M. A. F. Silva-Dia (2004), Smoking rain clouds over the Amazon, *Science*, 303, 1337–1342, doi:10.1126/science.1092779.
- Andreae, M., et al. (2001), Transport of biomass burning smoke to the upper troposphere by deep convection in the equatorial region, *Geophys. Res. Lett.*, 28, 951–954, doi:10.1029/2000GL012391.
- Arlander, D. W., D. Brüning, U. Schmidt, and D. H. Ehhalt (1995), The tropospheric distribution of formaldehyde during TROPOZ II, *J. Atmos. Chem.*, 22, 251–268, doi:10.1007/BF00696637.
- Baehr, J., H. Schlager, H. Ziereis, P. Stock, P. van Velthoven, R. Busen, J. Ström, and U. Schumann (2003), Aircraft observations of NO, NO<sub>y</sub>, CO, and O<sub>3</sub> in the upper troposphere from 60°N to 60°S—Interhemispheric differences at midlatitudes, *Geophys. Res. Lett.*, 30(11), 1598, doi:10.1029/2003GL016935.
- Barth, M. C., et al. (2007), Cloud-scale model intercomparison of chemical constituent transport in deep convection, *Atmos. Chem. Phys.*, 7, 4709–4731, doi:10.5194/acp-7-4709-2007.
- Barth, M. C., J. Lee, A. Hodzic, G. Pfister, W. C. Skamarock, J. Worden, J. Wong, and D. Noone (2012), Thunderstorms and upper troposphere chemistry during the early stages of the 2006 North American Monsoon, *Atmos. Chem. Phys.*, 12, 11,003–11,026, doi:10.5194/acp-12-11003-2012.
- Barth, M. C., et al. (2015), The Deep Convective Clouds and Chemistry (DC3) Field Campaign, *Bull. Am. Meteorol. Soc.*, 96, 1281–1309, doi:10.1175/BAMS-D-13-00290.1.
- Bela, M., et al. (2016), Wet Scavenging of Soluble Gases in DC3 Deep Convective Storms Using WRF-Chem Simulations and Aircraft Observations, *J. Geophys. Res. Atmos.*, 121, doi:10.1002/2015JD024623.
- Biggerstaff, M. I., L. J. Wicker, J. Guynes, C. L. Ziegler, J. M. Straka, E. N. Rasmussen, A. Doggett, L. D. Carey, J. L. Schroeder, and C. Weiss (2005), The Shared Mobile Atmospheric Research and Teaching radar: A collaboration to enhance research and teaching, *Bull. Am. Meteorol. Soc.*, 86, 1263–1274.
- Boegel, W., and R. Baumann (1991), Test and calibration of the DLR Falcon wind measuring system by maneuvers, *J. Atmos. Oceanic Technol.*, 8, 5–18, doi:10.1175/1520-0426(1991)008<0005:TACOTD>2.0.CO;2.
- Brooks, H. E. (2013), Severe thunderstorms and climate change, *Atmos. Res.*, 123, 129–138, doi:10.1016/j.atmosres.2012.04.002.
- Browell, E. V. (1989), Differential absorption lidar sensing of ozone, *Proc. IEEE*, 77, 419–432.
- Cecil, D. J. (2011), Relating passive 37-GHz scattering to radar profiles in strong convection, *J. Appl. Meteorol. Climatol.*, 50, 233–240, doi:10.1175/2010JAMC2506.1.
- Cecil, D. J., and C. B. Blankenship (2012), Toward a global climatology of severe hailstorms as estimated by satellite passive microwave imagers, *J. Clim.*, 25, 687–703, doi:10.1175/JCLI-D-11-00130.1.
- Chen, H., et al. (2010), High-accuracy continuous airborne measurements of greenhouse gases (CO<sub>2</sub> and CH<sub>4</sub>) using the cavity ring-down spectroscopy (CRDS) technique, *Atmos. Meas. Tech.*, 3, 375–386, doi:10.5194/amt-3-375-2010.
- Choi, Y., J. Kim, A. Elderling, G. Osterman, Y. L. Yung, and K. N. Liou (2009), Lightning and anthropogenic NO<sub>x</sub> sources over the U.S. and the western North Atlantic Ocean: Impact on OLR and radiative effects, *Geophys. Res. Lett.*, 36, L17806, doi:10.1029/2009GL039381.
- Cooper, O. R., et al. (2007), Evidence for a recurring eastern North America upper tropospheric ozone maximum during summer, *J. Geophys. Res.*, 112, D23304, doi:10.1029/2007JD008710.
- Cooper, O. R., et al. (2009), Summertime buildup and decay of lightning NO<sub>x</sub> and aged thunderstorm outflow above North America, *J. Geophys. Res.*, 114, D01101, doi:10.1029/2008JD010293.
- Cooper, O., et al. (2004), A case study of trans-Pacific warm conveyor belt transport: The influence of merging airstreams on trace gas import to North America, *J. Geophys. Res.*, 109, D23S08, doi:10.1029/2003JD003624.
- Crutzen, P. J. (1970), The influence of nitrogen oxides on the atmospheric ozone content, *Q. J. R. Meteorol. Soc.*, 96, 320–325, doi:10.1002/qj.49709640815.
- Crutzen, P. J. (1995), Overview of tropospheric chemistry: Developments during the past quarter century and a look ahead, in *Faraday Discussions on Atmospheric Chemistry—Measurements, Mechanics and Models*, vol. 100, pp. 1–21, R. Soc. Chem., Cambridge, doi:10.1039/FD9950000001.
- Cummings, K., et al. (2014), A WRF-Chem flash rate parameterization scheme and LNO<sub>x</sub> analysis of the 29–30 May 2012 convective event in Oklahoma during DC3, XV International Conference on Atmospheric Electricity, Norman, Okla, 15–20 June 2014, Oral Paper: O-11-08, 22 pp. [Available at <http://www.nssl.noaa.gov/users/mansell/icae2014/>]

- Cummins, K. L., and M. J. Murphy (2009), An overview of lightning locating systems: History, techniques, and data uses, with an in-depth look at the U.S. NLDN, *IEEE Trans. Electromagn. Compat.*, 51(3), 499–518.
- Dahlkötter, F., M. Gysel, D. Sauer, A. Minikin, R. Baumann, P. Seifert, A. Ansmann, M. Fromm, C. Voigt, and B. Weinzierl (2014), The Pagami Creek smoke plume after long-range transport to the upper troposphere over Europe—Aerosol properties and black carbon mixing state, *Atmos. Chem. Phys.*, 14, 6111–6137, doi:10.5194/acp-14-6111-2014.
- DeCaria, A. J., K. E. Pickering, G. L. Stenchikov, J. R. Scala, J. L. Stith, J. E. Dye, B. A. Ridley, and P. Laroche (2000), A cloud-scale model study of lightning-generated NO<sub>x</sub> in an individual thunderstorm during STERAO-A, *J. Geophys. Res.*, 105(D9), 11,601–11,616, doi:10.1029/2000JD900033.
- DeCaria, A. J., K. E. Pickering, G. L. Stenchikov, and L. E. Ott (2005), Lightning-generated NO<sub>x</sub> and its impact on tropospheric ozone production: A three-dimensional modeling study of a Stratosphere-Troposphere Experiment: Radiation, Aerosols and Ozone (STERAO-A) thunderstorm, *J. Geophys. Res.*, 110, D14303, doi:10.1029/2004JD005556.
- Dessler, A. E., and S. C. Sherwood (2004), Effect of convection on the summertime extratropical lower stratosphere, *J. Geophys. Res.*, 109, D23301, doi:10.1029/2004JD005209.
- Dickerson, R. R., et al. (1987), Thunderstorms: An important mechanism in the transport of air pollutants, *Science*, 235, 460–465, doi:10.1126/science.235.4787.460.
- Doherty, R. M., D. S. Stevenson, W. J. Collins, and M. G. Sanderson (2005), Influence of convective transport on tropospheric ozone and its precursors in a chemistry-climate model, *Atmos. Chem. Phys.*, 5, 3205–3218, doi:10.5194/acp-5-3205-2005.
- Draxler, R. R., and Rolph, G. D. (2014), HYSPLIT (HYbrid Single-Particle Lagrangian Integrated Trajectory) Model access via NOAA ARL READY Website, NOAA Air Resources Laboratory, Silver Spring, Md. [Available at <http://ready.arl.noaa.gov/HYSPLIT.php>.]
- Dye, J. E., et al. (2000), An overview of the Stratospheric-Tropospheric Experiment: Radiation, Aerosols, and Ozone (STERAO)-Deep Convection experiment with results for the July 10, 1996 storm, *J. Geophys. Res.*, 105(D8), 10,023–10,045, doi:10.1029/1999JD901116.
- Ehhalt, D. H., and F. Rohrer (1995), The impact of commercial aircraft on tropospheric ozone, in *The Chemistry of the Atmosphere—Oxidants and Oxidation in the Earth's Atmosphere, Spec. Publ. 7th BOC Priestley Conference*, vol. 170, edited by A. R. Bandy, pp. 105–120, The Royal Society of Chemistry, Lewisburg, Pa.
- Fischer, H., et al. (2003), Deep convective injection of boundary layer air into the lowermost stratosphere at midlatitudes, *Atmos. Chem. Phys.*, 3, 739–745, doi:10.5194/acp-3-739-2003.
- Fishman, J., S. Solomon, and P. J. Crutzen (1979), Observational and theoretical evidence in support of a significant in situ photochemical source of tropospheric ozone, *Tellus*, 31, 432–446, doi:10.1111/j.2153-3490.1979.tb00922.x.
- Gerbig, C., S. Schmitgen, D. Kley, A. Volz-Thomas, K. Dewey, and D. Haaks (1999), An improved fast-response vacuum-UV resonance fluorescence CO instrument, *J. Geophys. Res.*, 104, 1699–1704, doi:10.1029/1998JD100031.
- Hair, J. W., C. A. Hostettler, A. L. Cook, D. B. Harper, R. A. Ferrare, T. L. Mack, W. Welch, L. R. Izquierdo, and F. E. Hovis (2008), Airborne High Spectral Resolution Lidar for profiling aerosol optical properties, *Appl. Opt.*, 47, 6734–6752, doi:10.1364/AO.47.006734.
- Hegglin, M. I., et al. (2004), Tracing troposphere-to-stratosphere transport above a mid-latitude deep convective system, *Atmos. Chem. Phys.*, 4, 741–756, doi:10.5194/acp-4-741-2004.
- Holle, R. L., and M. J. Murphy (2015), Lightning in the North American monsoon: An exploratory climatology, *Mon. Weather Rev.*, 143, 1970–1977, doi:10.1175/MWR-D-14-00363.1.
- Homeyer, C. R., L. L. Pan, and M. C. Barth (2014), Transport from convective overshooting of the extratropical tropopause and the role of large-scale lower stratosphere stability, *J. Geophys. Res. Atmos.*, 119, 2220–2240, doi:10.1002/2013JD020931.
- Hudman, R. C., L. T. Murray, D. J. Jacob, S. Turquety, S. Wu, D. B. Millet, M. Avery, A. H. Goldstein, and J. Holloway (2009), North American influence on tropospheric ozone and the effects of recent emission reductions: Constraints from ICARTT observations, *J. Geophys. Res.*, 114, D07302, doi:10.1029/2008JD010126.
- Huntrieser, H., H. Schlager, C. Feigl, and H. Höller (1998), Transport and production of NO<sub>x</sub> in electrified thunderstorms: Survey of previous studies and new observations at midlatitudes, *J. Geophys. Res.*, 103, 28,247–28,264, doi:10.1029/98JD02353.
- Huntrieser, H., et al. (2002), Airborne measurements of NO<sub>x</sub>, tracer species and small particles during the European Lightning Nitrogen Oxides Experiment, *J. Geophys. Res.*, 107(D11), 4113, doi:10.1029/2000JD000209.
- Huntrieser, H., et al. (2005), Intercontinental air pollution transport from North America to Europe: Experimental evidence from airborne measurements and surface observations, *J. Geophys. Res.*, 110, D01305, doi:10.1029/2004JD005045.
- Huntrieser, H., H. Schlager, A. Roiger, M. Lichtenstern, U. Schumann, C. Kurz, D. Brunner, C. Schwierz, A. Richter, and A. Stohl (2007), Lightning-produced NO<sub>x</sub> over Brazil during TROCCINOX: Airborne measurements in tropical and subtropical thunderstorms and the importance of mesoscale convective systems, *Atmos. Chem. Phys.*, 7, 2987–3013, doi:10.5194/acp-7-2987-2007.
- Huntrieser, H., U. Schumann, H. Schlager, H. Höller, A. Giez, H.-D. Betz, D. Brunner, C. Forster, O. Pinto Jr., and R. Calheiros (2008), Lightning activity in Brazilian thunderstorms during TROCCINOX: Implications for NO<sub>x</sub> production, *Atmos. Chem. Phys.*, 8, 921–953, doi:10.5194/acp-8-921-2008.
- Huntrieser, H., et al. (2009), NO<sub>x</sub> production by lightning in Hector: First airborne measurements during SCOUT-O3/ACTIVE, *Atmos. Chem. Phys.*, 9, 8377–8412, doi:10.5194/acp-9-8377-2009.
- Huntrieser, H., H. Schlager, M. Lichtenstern, P. Stock, T. Hamburger, H. Höller, K. Schmidt, H.-D. Betz, A. Ulanovsky, and F. Ravagnani (2011), Mesoscale convective systems observed during AMMA and their impact on the NO<sub>x</sub> and O<sub>3</sub> budget over West Africa, *Atmos. Chem. Phys.*, 11, 2503–2536, doi:10.5194/acp-11-2503-2011.
- Huntrieser, H., H. Höller, and V. Grewe (2012), Thunderstorms: Trace species generators, in *Atmospheric Physics: Background-Methods-Trends Research Topics in Aerospace*, edited by U. Schumann, pp. 115–133, Springer, Berlin.
- Huntrieser, H., et al. (2016), On the origin of pronounced O<sub>3</sub> gradients in the thunderstorm outflow region during DC3, *J. Geophys. Res. Atmos.*, 121, doi:10.1002/2015JD024279.
- Jiang, J. H., et al. (2012), Evaluation of cloud and water vapor simulations in CMIP5 climate models using NASA "A-Train" satellite observations, *J. Geophys. Res.*, 117, D14105, doi:10.1029/2011JD017237.
- Jiang, J. H., H. Su, C. Zhai, L. Wu, K. Minschwaner, A. M. Molod, and A. M. Tompkins (2015), An assessment of upper troposphere and lower stratosphere water vapor in MERRA, MERRA2, and ECMWF reanalyses using Aura MLS observations, *J. Geophys. Res. Atmos.*, 120, 11,468–11,485, doi:10.1002/2015JD023752.
- Jourdain, L., S. S. Kulawik, H. M. Worden, K. E. Pickering, J. Worden, and A. M. Thompson (2010), Lightning NO<sub>x</sub> emissions over the USA constrained by TES ozone observations and the GEOS-Chem model, *Atmos. Chem. Phys.*, 10, 107–119, doi:10.5194/acp-10-107-2010.
- Konopka, P., J.-U. Groß, F. Plöger, and R. Müller (2009), Annual cycle of horizontal in-mixing into the lower tropical stratosphere, *J. Geophys. Res.*, 114, D19111, doi:10.1029/2009JD011955.
- Laborde, M., et al. (2012), Single Particle Soot Photometer intercomparison at the AIDA chamber, *Atmos. Meas. Tech.*, 5, 3077–3097, doi:10.5194/amt-5-3077-2012.

- Lang, T. J., S. A. Rutledge, B. Dolan, P. Krehbiel, W. Rison, and D. T. Lindsey (2014), Lightning in wildfire smoke plumes observed in Colorado during summer 2012, *Mon. Weather Rev.*, 142, 489–507, doi:10.1175/MWR-D-13-00184.1.
- Lawrence, M. G., and P. J. Rasch (2005), Tracer transport in deep convective updrafts: Plume ensemble versus bulk formulations, *J. Atmos. Sci.*, 62, 2880–2894, doi:10.1175/JAS3505.1.
- Lawrence, M. G., von Kuhlmann, R., Salzmann, M., and Rasch, P. J. (2003), The balance of effects of deep convective mixing on tropospheric ozone, *Geophys. Res. Lett.*, 30(18), 1940, doi:10.1029/2003GL017644.
- Leuchner, M., and B. Rappenglück (2010), VOC source-receptor relationships in Houston during TexAQS-II, *Atmos. Environ.*, 44, 4056–4067, doi:10.1016/j.atmosenv.2009.02.029.
- Liu, C., and E. J. Zipser (2015), The global distribution of largest, deepest, and most intense precipitation systems, *Geophys. Res. Lett.*, 42, 3591–3595, doi:10.1002/2015GL063776.
- Livesey, N., et al. (2011), EOS MLS version 3.3 level 2 data quality and description document Tech. Rep., Jet Propulsion Laboratory, California Institute of Technology, Pasadena, Calif.
- Lyons, W. A., T. E. Nelson, E. R. Williams, J. A. Cramer, and T. R. Turner (1998), Enhanced positive cloud-to-ground lightning in thunderstorms ingesting smoke from fire, *Science*, 282(5386), 77–80, doi:10.1126/science.282.5386.77.
- Minikin, A., A. Petzold, B. Weinzierl, and J.-F. Gayet (2012), In-situ measurement methods for atmospheric aerosol particles and cloud elements, in *Atmospheric Physics: Background-Methods-Trends Research Topics in Aerospace*, edited by U. Schumann, pp. 297–316, Springer-Verlag, Berlin Heidelberg.
- Murray, N. D., R. E. Orville, and G. R. Huffines (2000), Effect of pollution from Central American fires on cloud-to-ground lightning in May 1998, *Geophys. Res. Lett.*, 27, 2249–2252, doi:10.1029/2000GL011656.
- Myhre, G., et al. (2013), Anthropogenic and natural radiative forcing, in *Climate Change 2013: The Physical Science Basis. Contribution of Working Group I to the Fifth Assessment Report of the Intergovernmental Panel on Climate Change*, edited by T. F. Stocker et al., pp. 659–740, Cambridge Univ. Press, Cambridge, U. K., and New York, doi:10.1017/CBO9781107415324.018.
- Nault, B. A., C. Garland, S. E. Pusede, P. J. Wooldridge, K. Ullmann, S. R. Hall, and R. C. Cohen (2015), Measurements of  $\text{CH}_3\text{O}_2\text{NO}_2$  in the upper troposphere, *Atmos. Meas. Tech.*, 8, 987–997, doi:10.5194/amt-8-987-2015.
- Pan, L. L., et al. (2014), Thunderstorms enhance tropospheric ozone by wrapping and shedding stratospheric air, *Geophys. Res. Lett.*, 41, 7785–7790, doi:10.1002/2014GL061921.
- Pfister, G. G., L. K. Emmons, J. F. Hess, A. M. Thompson, and J. E. Yorks (2008), Analysis of the summer 2004 ozone budget over the United States using Intercontinental Transport Experiment Ozonesonde Network Study (IONS) observations and Model of Ozone and Related Tracers (MOZART-4) simulations, *J. Geophys. Res.*, 113, D23306, doi:10.1029/2008JD010190.
- Pickering, K. E., et al. (1996), Convective transport of biomass burning emissions over Brazil during TRACE A, *J. Geophys. Res.*, 101, 23,993–24,012, doi:10.1029/96JD00346.
- Ploeger, F., P. Konopka, R. Müller, S. Fueglistaler, T. Schmidt, J. C. Manners, J.-U. Grooß, G. Günther, P. M. Forster, and M. Riese (2012), Horizontal transport affecting trace gas seasonality in the Tropical Tropopause Layer (TTL), *J. Geophys. Res.*, 117, D09303, doi:10.1029/2011JD017267.
- Pollack, I. B., et al. (2016), Airborne quantification of upper tropospheric  $\text{NO}_x$  production from lightning in deep convective storms over the continental US, *J. Geophys. Res. Atmos.*, 121, 2002–2028, doi:10.1002/2015JD023941.
- Pollack, I. B., M. Lerner, and T. B. Ryerson (2010), Evaluation of ultraviolet light-emitting diodes for detection of atmospheric  $\text{NO}_2$  by photolysis—Chemiluminescence, *J. Atmos. Chem.*, 65, 111–125, doi:10.1007/s10874-011-9184-3.
- Potvin, C. K., D. Betten, L. J. Wicker, K. L. Elmore, and M. I. Biggerstaff (2012), 3DVAR versus traditional dual-Doppler wind retrievals of a simulated supercell thunderstorm, *Mon. Weather Rev.*, 140, 3487–3494, doi:10.1175/MWR-D-12-00063.1.
- Poulida, O., R. R. Dickerson, and A. Heymsfield (1996), Stratosphere-troposphere exchange in a midlatitude mesoscale convective complex. Part 1: Observations, *J. Geophys. Res.*, 101, 6823–6836, doi:10.1029/95JD03523.
- Randel, W. J., E. Moyer, M. Park, E. Jensen, P. Bernath, K. Walker, and C. Boone (2012), Global variations of HDO and HDO/H<sub>2</sub>O ratios in the upper troposphere and lower stratosphere derived from ACE-FTS satellite measurements, *J. Geophys. Res.*, 117, D06303, doi:10.1029/2011JD016632.
- Rappenglück, B., et al. (2006), The first VOC intercomparison exercise within the Global Atmosphere Watch (GAW), *Atmos. Environ.*, 40, 7508–7527, doi:10.1016/j.atmosenv.2006.07.016.
- Ray, E. A., et al. (2004), Evidence of the effect of summertime midlatitude convection on the subtropical lower stratosphere from CRYSTAL-FACE tracer measurements, *J. Geophys. Res.*, 109, D18304, doi:10.1029/2004JD004655.
- Read, W. G., et al. (2007), Aura Microwave Limb Sounder upper tropospheric and lower stratospheric H<sub>2</sub>O and relative humidity with respect to ice validation, *J. Geophys. Res.*, 112, D24535, doi:10.1029/2007JD008752.
- Ridley, B., et al. (2004), Florida thunderstorms: A faucet of reactive nitrogen to the upper troposphere, *J. Geophys. Res.*, 109, D17305, doi:10.1029/2004JD004769.
- Roach, W. T. (1967), On the nature of the summit areas of severe storms in Oklahoma, *Q. J. R. Meteorol. Soc.*, 93, 318–336, doi:10.1002/qj.49709339704.
- Rogers, R. R., et al. (2009), NASA LaRC airborne high spectral resolution lidar aerosol measurements during MILAGRO: Observations and validation, *Atmos. Chem. Phys.*, 9, 4811–4826, doi:10.5194/acp-9-4811-2009.
- Rolph, G. D. (2014), Real-time Environmental Applications and Display sYstem (READY) Website, NOAA Air Resources Laboratory, Silver Spring, Md. [Available at <http://ready.arl.noaa.gov/>.]
- Romps, D. M., J. T. Seeley, D. Vollaro, and J. Molinari (2014), Projected increase in lightning strikes in the United States due to global warming, *Science*, 346, 851–854, doi:10.1126/science.1259100.
- Schoeberl, M. R., A. E. Dessler, and T. Wang (2013), Modeling upper tropospheric and lower stratospheric water vapor anomalies, *Atmos. Chem. Phys.*, 13, 7783–7793, doi:10.5194/acp-13-7783-2013.
- Schroeder, J. R., L. L. Pan, T. Ryerson, G. Diskin, J. Hair, S. Meinardi, I. Simpson, B. Barletta, N. Blake, and D. R. Blake (2014), Evidence of mixing between polluted convective outflow and stratospheric air in the upper troposphere during DC3, *J. Geophys. Res. Atmos.*, 119, 11,477–11,491, doi:10.1002/jgrd.v119.19.
- Schultz, D. M., Y. P. Richardson, P. M. Markowski, and C. A. Doswell III (2014), Tornadoes in the Central United States and the “Clash of Air Masses”, *Bull. Am. Meteorol. Soc.*, 95, 1704–1712, doi:10.1175/BAMS-D-13-00252.1.
- Schumann, U., and H. Huntrieser (2007), The global lightning-induced nitrogen oxides source, *Atmos. Chem. Phys.*, 7, 3823–3907, doi:10.5194/acp-7-3823-2007.
- Schwartz, M. J., W. G. Read, M. L. Santee, N. J. Livesey, L. Froidevaux, A. Lambert, and G. L. Manney (2013), Convectively injected water vapor in the North American summer lowermost stratosphere, *Geophys. Res. Lett.*, 40, 2316–2321, doi:10.1002/grl.50421.

- Simmonds, P. G., A. J. Manning, R. G. Derwent, P. Ciais, M. Ramonet, V. Kazan, and D. Ryall (2005), A burning question. Can recent growth rate anomalies in the greenhouse gases be attributed to large-scale biomass burning events?, *Atmos. Environ.*, **39**, 2513–2517, doi:10.1016/j.atmosenv.2005.02.018.
- Speidel, M., R. Nau, F. Arnold, H. Schlager, and A. Stohl (2007), Sulfur dioxide measurements in the lower, middle and upper troposphere: Deployment of an aircraft-based chemical ionization mass spectrometer with permanent in-flight calibration, *Atmos. Environ.*, **41**, 2427–2437, doi:10.1016/j.atmosenv.2006.07.047.
- Stenchikov, G., R. Dickerson, K. Pickering, W. Ellis Jr., B. Doddrige, S. Kondragunta, O. Poulida, J. Scala, and W.-K. Tao (1996), Stratosphere-troposphere exchange in a mid-latitude mesoscale convective complex: Part 2. Numerical simulations, *J. Geophys. Res.*, **101**, 6837–6851, doi:10.1029/95JD02468.
- Stevenson, D. S., et al. (2006), Multimodel ensemble simulations of present-day and near-future tropospheric ozone, *J. Geophys. Res.*, **111**, D08301, doi:10.1029/2005JD006338.
- Turetsky, M. R., E. S. Kane, J. W. Harden, R. D. Ottman, K. L. Maines, E. Hoy, and E. S. Kashschke (2011), Recent acceleration of biomass burning and carbon losses in Alaskan forests and peatlands, *Nat. Geosci.*, **4**, 27–31, doi:10.1038/NGEO1027.
- Virts, K. S., J. M. Wallace, M. L. Hutchins, and R. H. Holzworth (2015), Diurnal and seasonal lightning variability over the Gulf Stream and the Gulf of Mexico, *J. Atmos. Sci.*, **72**, 2657–2665, doi:10.1175/JAS-D-14-0233.1.
- Wagner, T., J. Heland, M. Zöger, and U. Platt (2003), A fast H<sub>2</sub>O total column density product from GOME—Validation with in-situ aircraft measurements, *Atmos. Chem. Phys.*, **3**, 651–663, doi:10.5194/acp-3-651-2003.
- Wang, L., M. J. Newchurch, A. Pour-Biazar, S. Kuang, M. Khan, X. Liu, W. Koshak, and K. Chance (2013), Estimating the influence of lightning on upper tropospheric ozone using NLDN lightning data and CMAQ model, *Atmos. Environ.*, **67**, 219–228, doi:10.1016/j.atmosenv.2012.11.001.
- Wang, P. K. (2003), Moisture plumes above thunderstorm anvils and their contributions to cross-tropopause transport of water vapor in midlatitudes, *J. Geophys. Res.*, **108**(D6), 4194, doi:10.1029/2002JD002581.
- Wendisch, M., and J. L. Brenguier (Eds.) (2013), *Airborne Measurements for Environmental Research: Methods and Instruments*, pp. 655, Wiley-VCH Verlag GmbH & Co. KGaA, Weinheim, Germany.
- Xiao, Y., D. J. Jacob, and S. Turquety (2007), Atmospheric acetylene and its relationship with CO as an indicator of air mass age, *J. Geophys. Res.*, **112**, D12305, doi:10.1029/2006JD008268.
- Yang, Q., et al. (2015), Aerosol transport and wet scavenging in deep convective clouds: A case study and model evaluation using a multiple passive tracer analysis approach, *J. Geophys. Res. Atmos.*, **120**, 8448–8468, doi:10.1002/2015JD023647.
- Yuan, T., L. A. Remer, K. E. Pickering, and H. Yu (2011), Observational evidence of aerosol enhancement of lightning activity and convective invigoration, *Geophys. Res. Lett.*, **38**, L04701, doi:10.1029/2010GL046052.
- Ziereis, H., H. Schlager, P. Schulte, P. F. J. van Velthoven, and F. Slemr (2000), Distributions of NO, NO<sub>x</sub>, and NO<sub>y</sub> in the upper troposphere and lower stratosphere between 28° and 61°N during POLINAT 2, *J. Geophys. Res.*, **105**, 3653–3664, doi:10.1029/1999JD900941.
- Ziereis, H., et al. (2004), Uptake of reactive nitrogen on cirrus cloud particles during INCA, *Geophys. Res. Lett.*, **31**, L05115, doi:10.1029/2003GL018794.